SPATIAL CORRELATION ANALYSIS OF NIÑO3.4 SEA SURFACE TEMPERATURES WITH WESTERN NORTH AMERICA HYDROCLIMATE

by

Joshua P. Heyer

A thesis submitted to the faculty of
The University of Utah
in partial fulfillment of the requirements for the degree of

Master of Science

Department of Geography

The University of Utah

August 2016

Copyright © Joshua P. Heyer 2016

All Rights Reserved

The University of Utah Graduate School

STATEMENT OF THESIS APPROVAL

The thesis of **Joshua P. Heyer**

has been approved by the following supervisory committee members:

Simon Brewer	, Chair	**03/23/2016** Date Approved
Andrea Brunelle	, Member	**03/08/2016** Date Approved
Jacqueline Shinker	, Member	**03/03/2016** Date Approved

and by **Andrea Brunelle** , Chair/Dean of

the Department/College/School of **Geography**

and by David B. Kieda, Dean of The Graduate School.

ABSTRACT

The El Niño Southern Oscillation (ENSO) impacts hydroclimate variability in western North America (NA). Tropical Pacific sea-surface temperature (SST) forcing on NA hydroclimate has been explored in depth at regional-spatial scales. However, an understanding of how synoptic climate controls impact western NA hydroclimate headwaters at fine spatial resolutions over various seasons is needed. To accomplish this, grid-point correlation analyses were investigated between the El Niño Southern Oscillation 3.4 SST Index (Niño3.4) and monthly mean surface precipitation rate, 2-m temperature, and 500mb omega time-series data provided by the National Center for Environmental Prediction/North American Regional Reanalysis (NARR). Further, synoptic teleconnections were explored using grid-point correlation analysis between Niño3.4 SST and monthly mean 500mb geopotential height time-series data provided by the National Center for Environmental Prediction/National Center for Atmospheric Research (NCEP/NCAR) Global Reanalysis. Resulting spatial correlation patterns in this study are consistent with previous research both spatially and temporally that indicate strongest correlations occur for western NA during the winter (DJF). Correlations shown at a finer-scale spatial resolution afforded by the NARR product reveal distinct correlations in topographically complex watersheds in the intermountain U.S. west (IMW), with important implications for scarce water resources. Spatial analysis of correlation maps revealed seasonal correlation variability, multidecadal teleconnection

variability, and atmospheric vertical velocity correlations. Further, interannual hydroclimate variability was identified over important headwaters. An improved representation of Niño3.4 SST and western NA hydroclimate correlations demonstrates the NARR product as a viable option to explore recent western NA hydroclimate (1979 – present).

TABLE OF CONTENTS

LIST OF FIGURES

LIST OF ABBREVIATIONS

CONUS	Continental United States
DJF	December – February Winter Season
ENSO	The El Niño Southern Oscillation
GR	Global Reanalysis
IMW	Intermountain West
JJA	July – August Summer Season
MAM	March – May Spring Season
NA	North America
NARR	North American Regional Reanalysis
NCEP	National Center for Environmental Prediction
NCAR	National Center for Atmospheric Research
Niño3.4 SST	The El Niño Southern Oscillation 3.4 Sea-Surface Temperature Index
NOAA	National Oceanic and Atmospheric Administration
PDO	Pacific Decadal Oscillation
PNA	Pacific North American Pattern
SST	Sea-Surface Temperature
SOI	Southern Oscillation Index
SON	September – November Fall Season

ACKNOWLEDGMENTS

My desire to pursue a M.S. in Geography was realized as an undergraduate at the University of Wyoming. As a first-generation student, my journey into a graduate career began as a McNair scholar, working alongside Dr. J.J. Shinker on an undergraduate research project focused on drought in Wyoming. J.J. was instrumental to my acceptance of a National Science Foundation Graduate Fellowship, and her passion for climate research and higher education fueled my desire to continue on into a graduate career.

At the University of Utah, I have been fortunate to have worked with Dr. Simon Brewer and Dr. Andrea Brunelle. Both Simon and Andrea have been pivotal to my success during my master's, providing me with invaluable advice, support, and teaching me research skills needed for a successful career in academia.

I would like to thank the Department of Geography and the National Science Foundation for funding my master's thesis research, which explored questions I have pondered since my childhood. My research investigates how sea-surface temperature variability in the tropical Pacific Ocean impacts climate variability in western North America.

"This material is based upon work supported by the National Science Foundation Graduate Research Fellowship under Grant No. 1256065. Any opinion, findings, and conclusions or recommendations expressed in this material are those of the authors(s) and do not necessarily reflect the views of the National Science Foundation."

INTRODUCTION

Tropical Pacific sea-surface temperature (SST) forcing impacts hydroclimate variability globally in areas of the tropics and extratropics (Kiladis and Diaz 1989; Myneni et al. 1996; Trenberth et al. 1998; Verdon et al. 2004; Seager et al. 2005; Cane 2005). For western North America (NA), tropical Pacific SST forcing is known to effect hydroclimate variability (Ropelewski and Halpert, 1986; Cayan and Peterson 1989; Cayan 1996; Gershunov and Barnett 1998; Trenberth et al. 1998; Dettinger et al. 2000; Castro et al. 2001; Seager et al. 2005; Seager et al. 2012; Anderson 2012; Mills and Walsh 2013). Correlations are well established between tropical Pacific SST variability associated with El Niño/Southern Oscillation (ENSO) and western NA hydroclimate during the Northern Hemisphere winter season of December, January, and February (DJF), when precipitation in mountainous headwaters vital for water resources is observed (Wallace and Gutzler 1982; Kiladis and Diaz 1989; Cayan and Peterson 1989; Gershunov and Barnett 1998; Castro et al. 2001; Seager et al. 2005; Barron and Anderson 2010; Cook et al. 2010). ENSO forcing on extratropical atmospheric circulation variability in the northern Pacific Ocean (Wallace and Gutzler 1982; Kiladis and Diaz 1989; Graham and Barnett 1994), Rossby wave propagation (Chen and Newman 1998; Newman and Sardeshmukh 1998; Trenberth et al. 1998; Seager et al. 2005), and the meridional advection of subtropical moisture (Seager et al. 2005), can enhance or suppress cool season (i.e. October – March) and DJF precipitation and streamflow in western NA (Cayan and Peterson 1989; Gershunov and Barnett 1998; Dettinger et al.

2000; Castro et al. 2001; Seager et al. 2005; Barron and Anderson 2010; Cook et al. 2010). Atmospheric circulation anomalies responding to ENSO SST variability can result in regional climate extremes for western NA hydroclimate, such as persistent drought conditions experienced during the 1930s drought (Seager et al. 2005; Cook et al. 2010). Understanding the links between ENSO and western NA hydroclimate is therefore important for projections of water resources in this region.

Background

An improved spatial understanding of Niño3.4 SST and western NA hydroclimate is important when considering climate models for the 21st century, which predict arid conditions will intensify over southwestern NA in response to global warming (Seager et al. 2007; Seager and Vecchi 2010; Cook et al. 2014), decreasing surface water available for consumers in the region (Seager et al. 2012). This is supported by research indicating future reductions in seasonal-snow runoff are expected for western NA (Mote et al. 2005; Barnett et al. 2008; Milly et al. 2008; Pederson et al. 2011; Pierce and Cayan 2013). Further complicating water resources in western NA are uncertainties regarding future ENSO conditions (Cane 2005; Vecchi and Wittenberg 2010; Wittenberg et al. 2014; Yamazaki and Watanabe 2015). Our results provide an improved spatial understanding of western NA hydroclimate responses to Niño3.4 SST forcing, which can be used to evaluate the performance of climate models predicting future ENSO impacts on the region.

The strongest tropical Pacific SST and western NA hydroclimate correlations occur during the Northern Hemisphere DJF season (Wallace and Gutzler 1982; Kiladis and Diaz 1989; Graham and Barnett 1994; Gershunov and Barnett 1998, Seager et al.

2005), when snowfall important for mountain snowpack and water resources accumulates. This is supported by studies revealing strong correlations between the tropical Pacific and western NA hydroclimate during the cool season (Ropelewski and Halpert 1986; Redmond and Koch 1991; McCabe and Dettinger 1999; Cayan et al. 1999; Cook et al. 2010; Kirby et al. 2014). The Niño3.4 region of the central-tropical Pacific (170°W – 120°W, 5°N – 5°S) is known to have a strong influence on DJF extratropical atmospheric circulation in the northern Pacific, and the Niño3.4 SST Index has been widely used to investigate impacts on western NA hydroclimate (Cole and Cook 1998; Hu and Feng 2001; Cook et al. 2010; Mills and Walsh 2013; Coats et al. 2013). During an El Niño phase, wetter-than-normal DJF conditions typically occur in the southwestern U.S., and drier- than-normal conditions in the Pacific Northwest. During a La Niña phase, the reverse pattern is typically observed (Redmond and Koch 1991; Gershunov and Barnett 1998; McCabe and Dettinger 1999; Cayan et al. 1999; Cook et al. 2010; Kirby et al. 2014).

Our ability to forecast wet or dry conditions for western NA using Niño3.4 SST is complicated by nonstationary teleconnections (Cole and Cook 1998; McCabe and Dettinger 1999; Hu and Feng 2001; Coats et al. 2013). Paleo-sedimentary records suggest teleconnections are nonstationarity at century-to-millennial timescales (Clement et al. 2000; Moy et al. 2002; Barron and Anderson 2010; Anderson 2012; Antinao and McDonald 2013; Kirby et al. 2014; Liu et al. 2014; Wise and Dannenberg 2014). This is supported by reconstructions of teleconnection patterns over distinct time intervals using historical climate data and climate models, which indicate teleconnections are nonstationary on multidecadal timescales (Cole and Cook 1998; McCabe and Dettinger

1999; Hu and Feng 2001; Coats et al. 2013). Our results of Niño3.4 SST and 500mb geopotential height teleconnection during two distinct time intervals support previous studies that have identified multidecadal teleconnection variability.

Our understanding of synoptic teleconnection impacts on western NA surface hydroclimate is further affected by the complex terrain of the IMW, where topographic features influence climatic controls over spatially diverse seasonal precipitation maximums (Mock 1996; Shinker et al. 2006; Shinker and Bartlein 2010; Wise 2012). Spatial heterogeneity characterizes the timing of precipitation maximums in the IMW, which is a function of the varied topography influenced by large- and small-spatial scale climatic controls in the atmosphere and at the surface (Shinker et al. 2006; Shinker and Bartlein 2010). Because of this complexity, distinct correlation patterns in topographically complex headwater regions are identified and explored.

Additional indices used to explore western NA hydroclimate correlations are the Nino3 Index (Seager et al. 2005; Seager et al. 2010), the Southern Oscillation Index (SOI) (Redmond and Koch 1991; McCabe and Dettinger 1999; Cayan et al. 1999), the Pacific North American Pattern (PNA) (Wallace and Gutzler 1981; Yarnal and Diaz 1986; Leathers and Palecki 1992; Cayan 1996; Abatzoglou 2010), the North Atlantic Oscillation Index (Seager et al. 2010), and the Pacific Decadal Oscillation (PDO) (Mantua and Hare 2002; Newman et al. 2003; Mills and Walsh 2013). Changes in the SOI precede and directly impact ENSO SST variability (Trenberth Redmond and Koch 1991), while the PDO is thought to be interrelated to a combination of ENSO forcing (Newman et al. 2003; Mills and Walsh 2013) and the PNA pattern (Cayan 1996). The PNA (Wallace and Gutzler 1981) is an index of geopotential height variability (i.e. ridge-

trough patterns that dictate the position of subtropical and polar jet streams), controlling the delivery of winter season moisture to western NA (Yarnal and Diaz 1986). Tropical Pacific SST variability influences atmospheric patterns such as the PNA over the North Pacific Ocean and NA, with El Niño conditions generally associated with a positive PNA phase (Trenberth et al. 1998), resulting in lower snow water equivalents and drier winter conditions for mountainous western NA headwaters (Cayan 1996). Correlations between snow water equivalent (SWE) and Nino3 indicate the southward shift of storm tracks during El Niño events influence storm frequency, resulting in increased winter precipitation for southwestern NA (Seager et al. 2010). While our study only investigates Niño3.4 SST Index, tropical Pacific ENSO forcing on additional climate indices and synoptic patterns are important to consider, and are discussed in the previously mentioned studies.

Objectives

In this study, we attempt to improve our understanding of the link between Pacific SSTs and western NA hydroclimate by using grid-point correlations between Niño3.4 SST time series and key surface and atmospheric parameters. We use fine-scale NARR data to examine correlations in the topographically complex western NA headwaters, and investigate changes in teleconnection patterns over time using the NCEP-GR product. Specifically, the study has five main objectives:

1. Describe spatial patterns of correlations between Niño3.4 SST and western NA surface reanalysis variables (i.e. NARR precipitation rate and 2-m temperature);
2. Analyze how spatial patterns of correlations between Niño3.4 SST and western NA surface reanalysis variables vary seasonally;

3. Examine interannual DJF NARR precipitation variability over important western NA headwaters;
4. Investigate regional multidecadal teleconnection nonstationarity between two time periods (1948-1979 vs. 1979-2015), using NCEP-GR data (i.e. 500mb geopotential height); and
5. Explore Niño3.4 SST and 500mb atmospheric vertical velocity correlations over western NA (i.e. 500mb Omega).

Study Area

The study area is western NA, defined as areas west of 100° West, south of the US- Canada border, and north of 25° North. The spatial extent of precipitation, temperature, and 500mb omega maps encompasses the major headwater regions of western NA (i.e. Colorado River, Arkansas River, Columbia River, Missouri River, Snake River, Sacramento River, Gila River, Río Grande, and Río Conchos). Southwestern NA includes southwestern Colorado, southern Utah, southern Nevada, southern California, Arizona, New Mexico, and northern México. The U.S. IMW includes northern Nevada, Idaho, northern Utah, western Wyoming, western Montana, and northwestern Colorado. The Pacific Northwest consists of Washington, Oregon, and northern California. Maps of 500mb geopotential height encompass all of NA, and the northeastern Pacific Ocean. The northeastern Pacific is included, as synoptic teleconnection patterns of geopotential height over this region directly impact western NA hydroclimate variability.

DATA

We obtained NCEP/NCAR-GR monthly mean time-series data of 500mb geopotential height (m) from NOAA/ESRL Physical Science Division in Boulder, Colorado, USA (http://www.esrl.noaa.gov/psd/). NARR monthly mean time-series data (03/01/1979 – 02/01/2015) for surface-precipitation rate (kg/m^2/s), 2-m temperature, and 500mb omega (Pascal/s) were obtained from the same source. The grid size of the NARR product is much finer than the NCEP-GR product (0.3°x0.3° vs. 2.5°x2.5°, respectively) (Mesinger et al. 2006). An explanation of NARR variables precipitation rate and 2-m temperature is provided in the Appendix, and additional information can be found at http://www.emc.ncep.noaa.gov/mmb/rreanl/.

Niño3.4 SST monthly mean and monthly anomaly data are provided by the Working Group on Surface Pressure at http://www.esrl.noaa.gov/psd/gcos_wgsp/Timeseries/Nino34/. Niño3.4 SST data provided by the Working Group on Surface Pressure is from the NOAA Earth System Research Laboratory Physical Science Division via the HadISST1 dataset (Rayner et al. 2003). Southern Oscillation Index (SOI) monthly sea-level pressure anomaly data are provided by the Working Group on Surface Pressure at http://www.esrl.noaa.gov/psd/gcos_wgsp/Timeseries/SOI/. Monthly mean Pacific North American Index (PNA) data are provided by the NOAA Climatic Prediction Center at http://www.esrl.noaa.gov/psd/data/climateindices/list/.

METHODS

Correlations were explored via grid-point correlations between Niño3.4 SST and hydroclimate variables provided by the NCEP-GR product (Kalnay et al. 1996; Kistler et al. 2001), and the NARR product (Mesinger et al. 2006). The NARR is a coupled land-atmosphere model that provides additional data over NA at finer spatial and temporal resolutions compared to NCEP-GR data (Mesinger et al. 2006). The 500mb level was chosen for atmospheric variables NCEP-GR geopotential height and NARR omega. The 500mb geopotential height level detects ridges and troughs, while the 500mb omega level detects vertical rising or subsiding motions.

Table 1 lists the set of correlations performed in R (R 2015) between different climate indices and reanalysis variables, and the seasons. For each set of correlations, a time series was created for the appropriate season for both Niño3.4 SST, and NCEP-GR and NARR climate variables at each grid. Correlations were then estimated using Pearson's coefficient, with a standard transformation to a t-statistic to assess significance (p-value < 0.05). Resulting Pearson's correlation coefficients and p-values were then interpolated using the Akima package (Akima 1978**)** onto a regular 0.3° x 0.3° latitude and longitude grid in R (R 2015) for consistency with the NARR (0.3° x 0.3° grid spacing). Resulting correlation coefficient and p-value grids were then mapped in Panoply NetCDF viewer, a data visualization tool for NetCDF file formats (http://www.giss.nasa.gov/tools/panoply/).

Seasons Selection

The selection of Niño3.4 SST for all grid-point correlation analyses in our study is justified based on results from previous studies. During the cool season (i.e. October – March), strong correlations have been established between tropical Pacific SST, the PNA, and western NA hydroclimate (Yarnal and Diaz 1986; Leathers and Palecki 1992; Cayan 1996; Trenberth et al. 1998; Abatzoglou 2010). Further, correlations between SOI and western NA hydroclimate have been explored (Redmond and Koch 1991; McCabe and Dettinger 1999). More recently, the Niño3.4 SST Index has been used to investigate central tropical Pacific forcing on western NA hydroclimate (e.g. Coats et al. 2013). For the purpose of our study, grid-point correlation analysis for the cool season was performed between SOI monthly sea-level pressure anomalies (June – November**)**, monthly PNA anomalies (October – March), and monthly mean NARR surface precipitation rate (October – March). Resulting grid-point correlation maps were then spatially compared to the cool season Niño3.4 SST and precipitation rate correlation map. Correlations were seemingly analogous between the cool season Niño3.4 SST and precipitation rate correlation map and the SOI and precipitation rate correlation map. Correlations were overall weaker over western NA using the PNA (Supplementary Figure 1). The impact of Niño3.4 SST on western NA hydroclimate is the focus of this study, and therefore, no additional grid-point correlations using SOI and PNA were performed. SOI and PNA correlation maps for the cool season are included in the Appendix.

Three-month time intervals (i.e. December – February (DJF); March – May (MAM); June – August (JJA); and September – November (SON)) are used to analyze

seasonal correlation variability (Graham and Barnett 1994; Gershunov and Barnett 1998). As previous studies indicate, Niño3.4 SST is a dominant forcing on atmospheric circulation and moisture transport to western NA during DJF (e.g. Graham and Barnett 1994; Seager et al. 2005). Therefore, the DJF season is the main focus of our study. We also explore correlations during the cool (i.e. October – March) and warm seasons (i.e. April – September), based on previous studies using the cool and warm seasons to explore Pacific SST impacts on the water year and growing season (Redmond and Koch 1991; McCabe and Dettinger 1999; Cayan et al. 1999; Cook et al. 2010).

Interannual Hydroclimate Variability

To investigate interannual hydroclimate variability within important upper headwaters, grid-point time series of mean monthly NARR precipitation-rate (DJF) data with mean monthly Niño3.4 SST (Nov – Mar) were constructed from 1979 – 2015. NARR precipitation rate data used in time-series analysis was obtained from grid cells located over important headwaters (i.e. Snake/Missouri River, Colorado River, Gila River, and Sacramento River). To identify anomalous precipitation years for selected NARR grid cells, mean-monthly NARR precipitation rate (DJF) values were scaled to a zero mean, and standard deviation values where calculated in R relative to the long-term mean (DJF; 1979 – 2015) (R 2015). Niño3.4 SST values were also scaled to a zero mean, and standard deviation values were calculated in R relative to the long-term mean (NDJFM; 1979 – 2015) (R 2015). Scaled and standardized NARR precipitation rate values were then plotted with scaled and standardized Niño3.4 SST values. Anomalous DJF precipitation years were identified when mean NARR DJF surface-precipitation rate were outside +/- 1 standard deviation (sd). Anomalous Niño3.4 SST years were identified

when Niño3.4 SST were outside of +/- 1sd for five consecutive months over DJF. Years were then recognized when Niño3.4 SST anomalies +/- 1sd coincided with DJF precipitation +/- 1sd. For all four headwaters, years of significant coinciding NARR precipitation and Niño3.4 SST anomalies were determined.

Multidecadal Teleconnection Nonstationarity

Following our investigation of seasonal correlation variability and interannual hydroclimate variability, multidecadal teleconnection nonstationarity over DJF was explored using the NCEP-GR product. Multidecadal teleconnection nonstationarity over DJF was investigated using 500mb geopotential height data. Grid-point calculations were calculated for two periods (e.g. DJF; 1948 – 1979 and 1979 – 2015). Two time periods were chosen based on a previous study using geopotential height to explore multidecadal teleconnection nonstationarity (e.g. Coats et al. 2013). The duration of the latter period (1979 – 2015) was chosen to provide temporal consistency with the NARR dataset and correlations.

Table 1. Correlations performed between reanalysis variables and climate indices. Seasons when correlations were performed are indicated (e.g. DJF)

	Niño3.4 SST	SOI	PNA
NARR Surface Precipitation Rate (kg/m^2/sec)	DJF, MAM, JJAS, Cool Season, Warm Season	Cool Season	Cool Season
NARR 2-m Temperature	DJF, MAM, JJAS, Cool Season, Warm Season	N/A	N/A
NARR 500mb Omega (Pascal/s)	DJF	N/A	N/A
GR NCEP/NCAR 500mb Geopotential Height (m)	DJF	N/A	N/A

RESULTS

Grid-point correlation analyses between Niño3.4 SST and reanalysis variables (Table 1) reveal spatial and temporal variability in western NA climate associated with SST anomalies. The results show seasonal correlation variability (Figure 1 – Figure 4), and interannual precipitation variability over important headwaters during DJF (i.e. Snake/Missouri River, Colorado River, Gila River, Sacramento River) (Figure 5). Further, multidecadal teleconnection nonstationarity is observed between two periods (i.e. DJF; 1948 – 1979 and 1979 – 2015) using GR 500mb geopotential height data (Figure 6). Finally, our results demonstrate the impact of Niño3.4 SST on atmospheric vertical velocity over western NA (Figure 7).

Spatial Patterns of Correlations

Figure 1 and Figure 2 show Niño3.4 SST and NARR surface precipitation correlations in western NA during the selected seasons. Positive correlations indicate wetter conditions are the typical response to positive Niño3.4 SST, and drier conditions are the typical response to negative Niño3.4 SST. Negative correlations indicate wetter conditions are the typical response to negative Niño3.4 SST, and drier conditions are the typical response to positive Niño3.4 SST. Significant correlations (p-value < 0.05) are spatially cohesive over southwestern NA during the cool season, DJF, and MAM, and considerably reduced, in comparison, during the warm season, JJA, and SON (Figure 1 – Figure 2).

Consistent with previous work, a correlation dipole is observed during the cool season (Figure 1A and 1B) and DJF (Figure 2A and 2B). We define the dipole as oppositely signed correlations between the northern and southern portions of western NA shown on the correlation maps. Significant positive correlation values are widespread over southwestern NA, while significant negative correlation values are restricted to areas of the northern IMW during the cool season (Figure 1A and 1B) and DJF (Figure 2A and 2B). However, much of the areas between the correlation dipole are not statistically significant, including the central-northern Great Basin, the greater part of the IMW north of Arizona and New México, the Pacific Northwest, the northern Sierra Nevada Mountains, and the Cascade Mountains.

Grid-point correlation maps for MAM (Figure 2C and 2D) reveal significant positive correlations concentrated over southwestern NA. Additional areas of significant positive correlations are observed over a small region of western Colorado near the Green River, northwestern Nevada, and southeastern Oregon. Positive correlations (not statistically significant) extend north into Oregon, southern Idaho, southern Wyoming, the Great Basin, western Colorado, and eastern Utah. Weak positive correlations (not statistically significant) appear over the Colorado River headwaters, and weaker positive and negative correlations are found over the Snake River and Missouri River headwaters in northwestern Wyoming, and the Pacific Northwest.

During the warm season (Figure 1C and 1D) and JJA (Figure 2E and 2F), significant positive correlations are seen extending from northeastern Nevada to southern Montana. Areas of significant positive correlations are found over the borders of northwestern Utah, southern Idaho and northeastern Nevada, northwestern and central

Wyoming, south-central Montana, and south- central Oregon. Significant negative correlations during the warm season and JJA are confined to areas of northwestern, central, and southeastern Arizona, extreme southeastern Nevada, and extreme southwestern New Mexico. Weak positive and negative correlations (not statistically significant) are widespread over western NA. Overall, correlations are stronger during JJA compared to the warm season.

Significant positive correlations during SON (Figure 2G and 2H) are observed over concentrated areas of Southern-central California, the northern portion of South Baja California, across western and eastern Utah, western central Colorado, and central New Mexico. Significant negative correlations are concentrated over a small area in the Cascade Mountains of central Oregon. Overall weaker correlations (statistically significant) are observed across the majority of western NA during SON.

Figure 3 and Figure 4 illustrate Niño3.4 SST and NARR 2-m temperature correlations in western NA. Positive correlations indicate warmer-than-normal land surface temperatures are the typical response to positive Niño3.4 SST, while cooler-than-normal surface temperatures are the typical response to negative Niño3.4 SST. Negative correlations indicate warmer-than-normal land surface temperatures are the typical response to negative Niño3.4 SST, while cooler-than- normal land surface temperatures are the typical response to positive Niño3.4 SST. Significant correlations are limited to the Pacific Northwest, and central Mexico into Texas (in spring) over western NA during the cool season, DJF, and MAM. During the cool season, DJF, and MAM, a dipole is observed, with positive correlations over northwestern U.S., and negative correlations over southwestern NA. During the warm season, JJA, and SON, significant correlations

are not observed over western NA, with the exception of extreme western Oregon Washington (Figure 3).

During the cool season, a correlation dipole is observed over western NA (Figure 3A and 3B). Significant positive correlations are found in the northwestern U.S., including western and southern Idaho, northern California (Sacramento River headwaters), northwestern Nevada, and all of Oregon and Washington. Significant negative correlations are found in southwestern NA including eastern-southern New Mexico and localized areas of Arizona, but are largely centered on northern México east of the Sierra Madre Occidental Mountains (Río Conchos watershed). Weaker correlations (not statistically significant) are observed between the correlation dipole including northern Arizona, Utah, Colorado, southern Wyoming, the Great Basin, and central-southern California.

Significant positive DJF correlations extend over the Columbia River, Missouri River, Snake River, and Sacramento River headwaters, in addition to the northern Wasatch Range headwaters in Utah (Figure 4A and 4B). Significant negative correlations are observed in Central Mexico over the Río Conchos watershed, México, for both the cool season and DJF. Weak positive and negative DJF correlations (not statistically significant) are identified between the dipole boundary, including central-southern California, south-central Nevada, Arizona, south- central Utah, southern Wyoming, Colorado, New Mexico, and areas west of the Sierra Madre Occidental Mountains in México.

During MAM, significant positive correlations are concentrated over the Pacific Northwest (Figure 4C and 4D). Significant negative correlations extend over northern

México, New Mexico, Texas, southeastern Arizona, and localized areas of southern California, Utah, and Colorado. Weaker correlations are observed over California, Utah, and southern most Colorado.

Weak negative correlations (not statistically significant) are widespread over much of western NA during JJA (Figure 4E and 4F) and the warm season (Figure 3C and 3D). Significant positive correlations are spatially restricted to extreme southwestern Washington and Oregon. Significant negative correlations are not observed in western NA.

Similar to JJA, weak negative correlations are widespread across all of western NA during SON, with the exception of weak positive correlations over western California and the Pacific Northwest (Figure 4G and 4H). Significant positive correlations are restricted to extreme southwestern Washington. Significant negative correlations are widespread over eastern Colorado, eastern New Mexico, and northwestern Texas.

Seasonal Correlation Variability

Spatial analysis of Niño3.4 SST and NARR precipitation correlations between seasons demonstrate seasonal correlation variability over western NA (Figure 1 and Figure 2). Our results identify a seasonal correlation dipole reversal between the cool/DJF and warm/JJA seasons. However, not all correlations are significant. In fact, the only significant correlations that are widespread over southwestern NA are during the cool/DJF seasons. The opposite is true for areas of the IMW, northern Idaho, northwestern Montana, and northwestern Wyoming (i.e. negative correlations during cool/DJF season; positive correlations during warm/JJA season), but these correlations are not statistically significant. Following the warm/JJA season, the correlation dipole

reverses during SON to correlation spatial patterns similar to DJF (i.e. overall negative correlations over the northwestern U.S.; overall positive correlations over southwestern NA), but largely not significant.

A comparison spatially of correlation strength indicates significant positive correlations are more extensive over western NA during the cool season compared to DJF (Figure 1A and Figure 2A), extending into southern Utah and southwestern Colorado (with exception of the Sacramento watershed). Opposite to positive correlations, negative correlations are stronger during DJF compared to the cool season. Compared to the cool season, DJF negative correlations have a larger spatial extent over the Colorado River, Columbia River, Missouri River, and Snake River headwaters, in addition to the Arkansas River headwaters.

MAM correlations (Figure 2C and 2D) compared spatially to DJF correlations (Figure 2A and 2B) reveal significant positive correlations further concentrated over southwestern NA. The correlation dipole is unobservable over western NA, as DJF negative correlations are replaced by weak positive correlations during MAM that are not statistically significant. MAM positive correlations compared to DJF positive correlations extend further north into Oregon, southern Idaho, southern Wyoming, the Great Basin, western Colorado, and eastern Utah. Opposite to DJF correlations, weak positive correlations appear over the Colorado River headwaters during MAM. Significant negative correlations found in the Missouri River and Snake River headwaters during DJF become weaker positive and negative correlations during MAM. Overall, Niño3.4 SST and NARR precipitation positive correlations shift northward during MAM compared to DJF.

Correlations weaken, and become spatially constricted during the warm season (Figure 1C and 1D) and JJA (Figure 2E and 2F) compared to the cool season, DJF, and MAM. Overall, correlations are stronger during JJA compared to the warm season, but lack overall significance for both JJA and warm season. Further, a correlation dipole reversal occurs between DJF and JJA (e.g. negative correlations over southwestern NA; positive correlations over the northwestern U.S.), but the correlation dipole pattern during JJA lacks significance compared to DJF (Figure 1A and D).

Compared to the cool season, DJF, and MAM, significant SON correlations are weaker and spatially restricted (Figure 2G and 2H). However, for Utah and areas of western Colorado, significant positive correlations are spatially extensive and the strongest during SON compared to all other seasons. Overall, spatial patterns of correlations during SON illustrate weak negative correlations over the northwestern U.S., and weak positive correlations over southwestern NA.

Analogous to Niño3.4 SST and NARR precipitation correlations, a comparison of Niño3.4 SST and 2-m temperature correlations between seasons reveals seasonal correlation variability over western NA. However, dissimilar to the Niño3.4 SST and NARR precipitation seasonal correlation is the absence of a seasonal correlation dipole reversal for Niño3.4 SST and 2-m temperature correlations. Rather, the correlation dipole shifts northward from DJF (Figure 4A and 4B) to MAM (Figure 4C and 4D). Overall, a clear correlation dipole is not observed during JJA or SON, with weak negative correlations over most of western NA (excluding northern México during JJA that are not statistically significant), and restricted areas of positive correlations over western California, Washington, and Oregon.

Differences are observed between the cool season (Figure 3A and 3B) and DJF (Figure 4A and 4B) correlation values. Compared to the cool season, DJF positive correlations are stronger and extend further inland over the northern IMW into the Snake River and Missouri River headwaters. Significant negative correlations are weaker during DJF and less prevalent over southwestern NA compared to the cool season.

A comparison of DJF and MAM correlation maps illustrate seasonal correlation variability. Spatial patterns of correlations shift during MAM (Figure 4C and 4D). Significant positive correlations are more concentrated over the Pacific Northwest, while negative correlations strengthen, move north, and extend over northern México, New Mexico, Texas, southeastern Arizona, and southern Colorado.

Similar to Niño3.4 SST and precipitation correlations, Niño3.4 SST and 2-m temperature correlations are weakest during the warm season (3C and 3D), and JJA (Figure 4E and 4F) and lack statistical significance in JJA. From MAM to the warm season and JJA, correlations weaken, and a clear correlation dipole is unobservable and lack statistical significance. Further, significant correlations occur during MAM restricted to northern México, western Washington, and Oregon during the warm season and JJA.

Spatial correlation patterns during SON (Figure 4G and 4H) are analogous to JJA, with the exception of northern México, eastern Colorado and New Mexico, and northwestern Texas. Negative correlations replace positive JJA correlations over northern México during SON. Over eastern Colorado, eastern New Mexico, and northwestern Texas, significant negative correlations are spatially extensive.

Interannual Hydroclimate Variability

Interannual DJF precipitation variability is observed for all four headwater grid-point time series of Niño3.4 SST and DJF precipitation anomalies (Figure 5). For the Snake/Missouri River headwaters, five significant anomalous years (i.e. Niño3.4 SST and surface precipitation +/- 1sd) responded to Niño3.4 SST as expected based on DJF correlation maps (gray dotted vertical line), and one significant anomalous year responded to Niño3.4 SST not as expected (red dotted vertical line) (Figure 5A). For the Colorado River headwaters, six significant anomalous years responded to Niño3.4 SST as expected (gray dotted vertical line), and two significant anomalous years responded to Niño3.4 SST not as expected (red dotted vertical line) (Figure 5B). Analysis of the Gila River headwaters reveals four significant anomalous years responded to Niño3.4 SST as expected (gray dotted vertical line), and one significant anomalous year responded to Niño3.4 SST not as expected (red dotted vertical line) (Figure 5C). The Sacramento River headwaters time series shows no clear response to Niño3.4 SST forcing, as expected based on DJF precipitation correlation maps (Figure 5D). For the Sacramento headwaters, anomalous years are indicated (gray dotted vertical line).

Multidecadal Teleconnection Nonstationarity

Figure 6 demonstrates multidecadal teleconnection nonstationarity during DJF over NA, and the northeastern Pacific Ocean. A comparison of Niño3.4 SST and 500mb geopotential height correlation maps and p-value maps during DJF for time periods 1948 – 1979 (Figure 6A and 6B), and 1979 – 2015 (Figure 6C and 6D), reveal areas of significant synoptic teleconnection nonstationarity.

During DJF from 1948 – 1979, significant positive correlations are found over

central- western Canada, central to southern México into South America, and the tropical Pacific (Figure 6A and 6B). Significant negative correlations are found over the southeastern U.S., and over a concentrated area of the northeastern Pacific, adjacent to the western U.S. coast (Figure 6A and 6B). During DJF from 1979 – 2015, significant positive correlations are seen over Central America into South America, and the tropical Pacific Ocean. Significant negative correlations are observed over the southwestern U.S., northern México, and most of the northeastern Pacific.

When comparing DJF spatial patterns of teleconnections from 1948 – 1979 to 1979 – 2015, a teleconnection shifts occur (Figure 6). Significant positive DJF correlations over the equatorial Pacific Ocean, central-southern México, and the Caribbean from 1948 – 1979 shift to a more southerly position from 1979 – 2015. Positive correlations over central-western Canada weaken, and shift eastward from 1948 – 1979 to 1979 – 2015. Significant negative DJF correlations over the southeastern U.S. weaken from 1948 – 1979, shift westward, and strengthen over southwestern NA from 1979 – 2015. Over the northeastern Pacific Ocean, negative correlations expand and strengthen from 1948 – 1979 to 1979 – 2015.

It can be inferred that the associated subtropical and polar jet streams respond to shifts in the strength and position of Niño3.4 SST and 500mb geopotential height correlations during DJF from 1948 – 1979 to 1979 – 2015. An example of this, significant correlations over the tropical Pacific shift south from 1948 – 1979 to 1979 – 2015, and subtropical flow becomes more meridional. The phase change from a negative PDO phase (1951 – 1975) to a positive PDO phase (1977 – 2001) (Mills and Walsh 2013) could be an underlying regional control on multidecadal teleconnection

nonstationarity observed in our study. Multidecadal teleconnection nonstationarity impacts the position of the subtropical and polar jet streams, which impacts where moisture for precipitation is delivered. The impacts of multidecadal teleconnection non-stationarity on the position of the jet streams and moisture delivery is explored in the discussion section.

Atmospheric Vertical Velocity Correlations

Niño3.4 SST and NARR 500mb omega DJF correlations are found in Figure 7A. Positive correlations show rising motions (500mb) associated with negative Niño3.4 SST, and sinking motions (500mb) associated with positive Niño3.4 SST. Negative correlations reveal rising motions (500mb) associated with positive Niño3.4 SST, and sinking motions (500mb) associated with negative Niño3.4 SST. Areas of significant correlations are shown (Figure 7B). DJF correlation and p-value maps for 500mb omega show significant positive correlations over high-elevation areas of western NA important for winter snowpack and water resources: Colorado Platea, western Colorado and eastern Utah; Great Divide Basin, Wyoming; and the Rocky Mountains, northwestern Montana.

Significant negative DJF correlations for 500mb omega are found in high-elevations of western NA: Rocky Mountains east of the Continental Divide, Colorado and Wyoming; Big Horn Mountains, Wyoming; northwestern Black Hills, South Dakota; Sawtooth Range, Idaho; Brian Head, and the eastern Uinta Mountains, Utah; Schell Creek Range, Nevada; Cascade Range, Oregon and Washington; Klamath Range, California; Mogollon Ridge and San Francisco Mountains, Arizona; Zuni Mountains and San Francisco Mountains, New Mexico. Significant negative correlations dominate the eastern Pacific Ocean along the western U.S. coast.

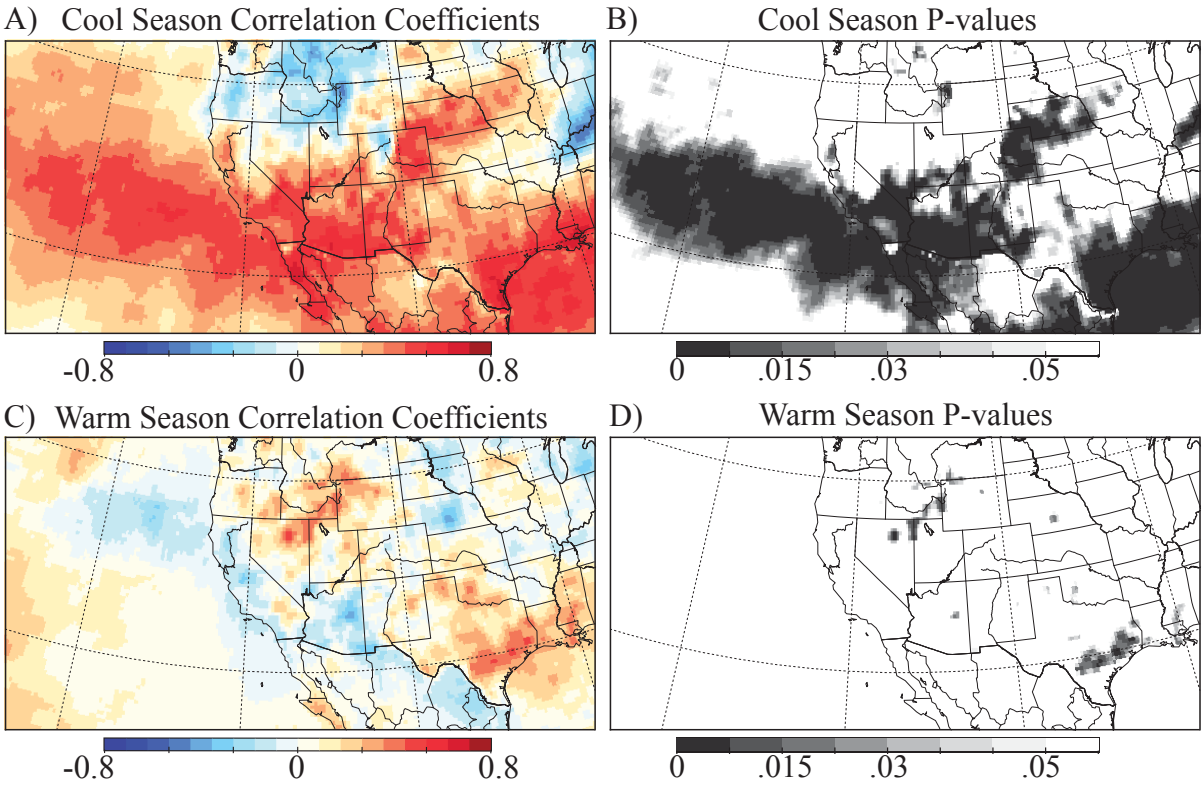

Figure 1: Pearson's correlation coefficients and p-value maps calculated between Niño3.4 SST and NARR surface-precipitation rate (03/1979 - 09/2015). Maps represent mean correlations and p-values for the cool season (A-B; October – March), and the warm season (C-D; April – September).

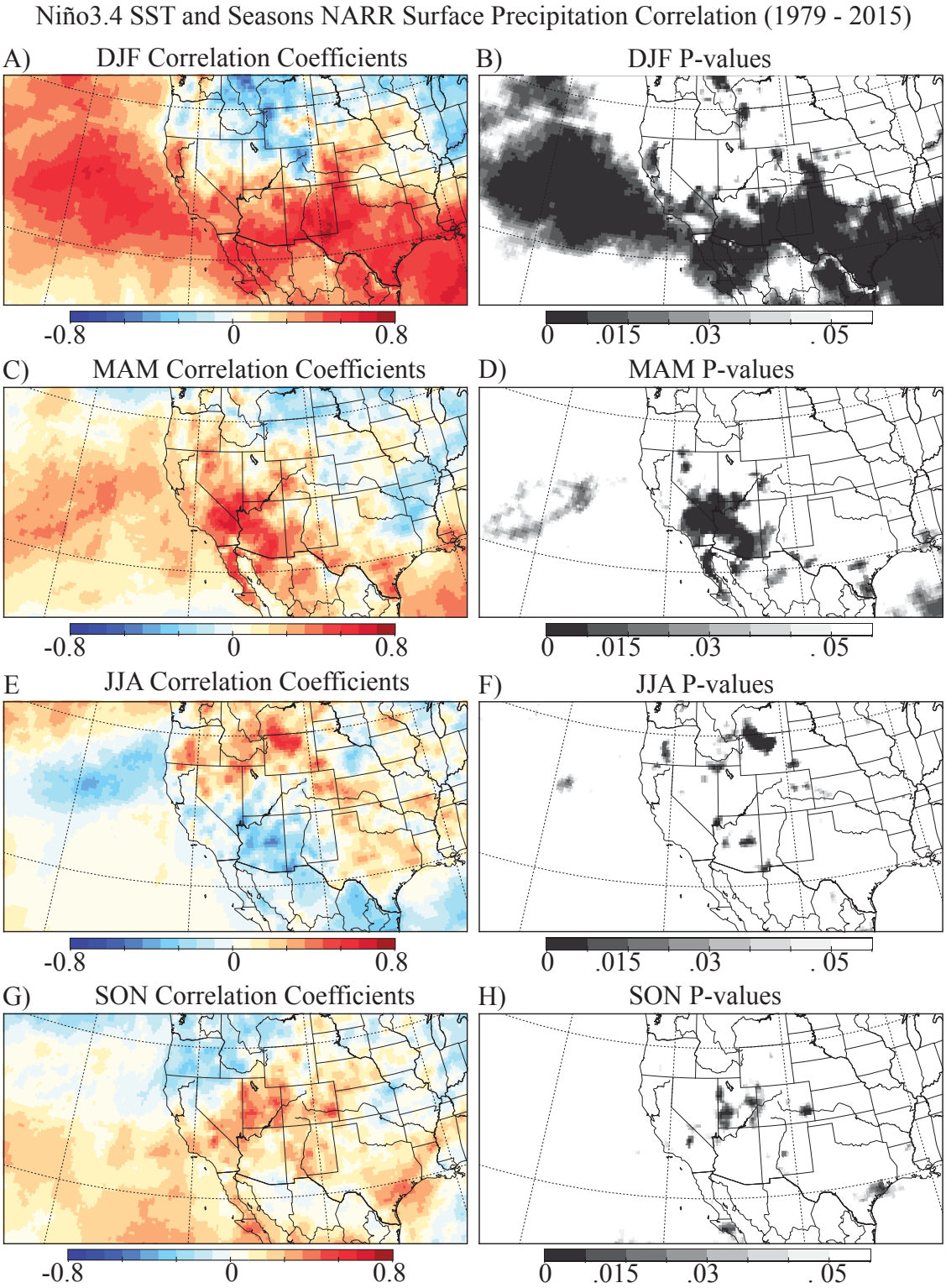

Figure 2: Niño3.4 SST and NARR surface precipitation rate correlation and p-value maps (03/1979 - 11/2015). Correlation and p-value maps are for the winter (A-B; December - February), spring (C-D; March - May), summer (E-F; June - August), and fall (G-H; September - November). Areas of significant correlations (p-value < 0.05) are shaded light to dark gray.

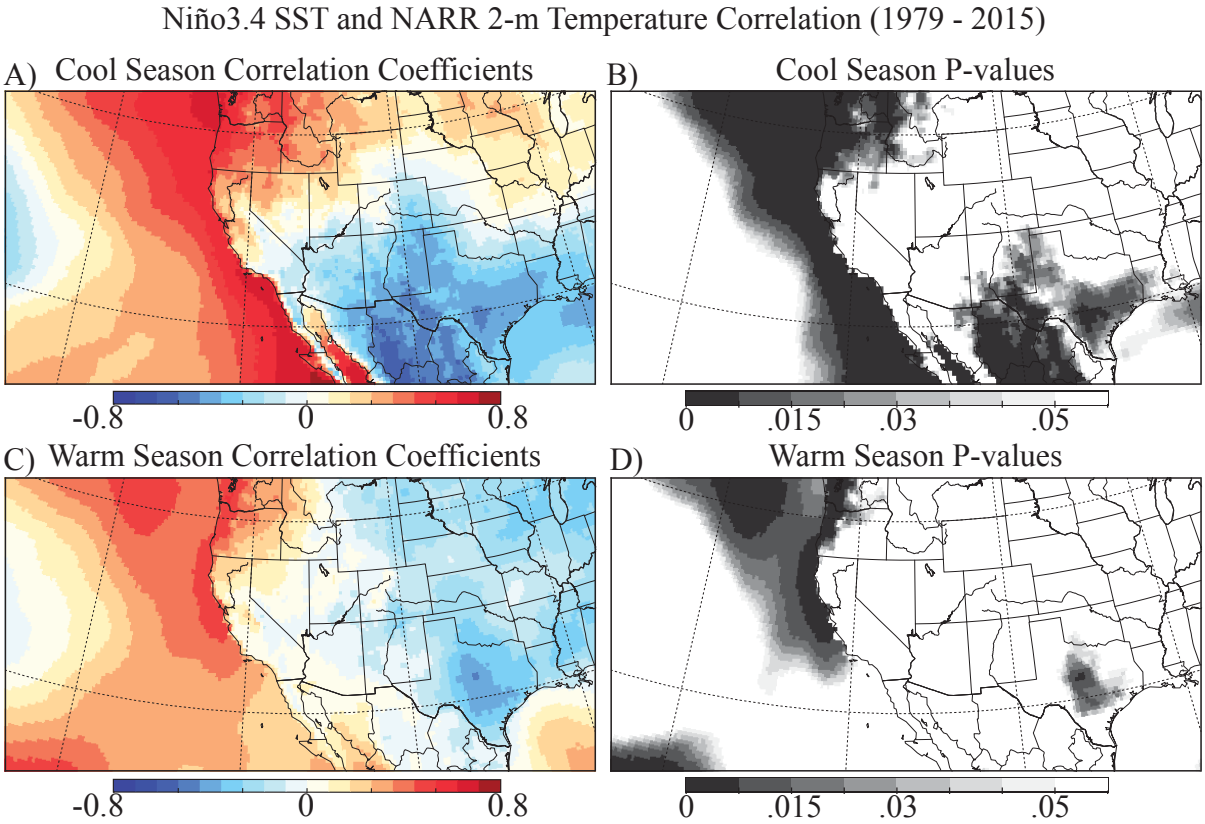

Figure 3: Pearson's correlation coefficients and p-value maps calculated between Niño3.4 SST and NARR 2-m temperature (03/1979 - 09/2015). Maps represent mean correlations and p-values for the cool season (A-B; October – March), and the warm season (C-D; April – September).

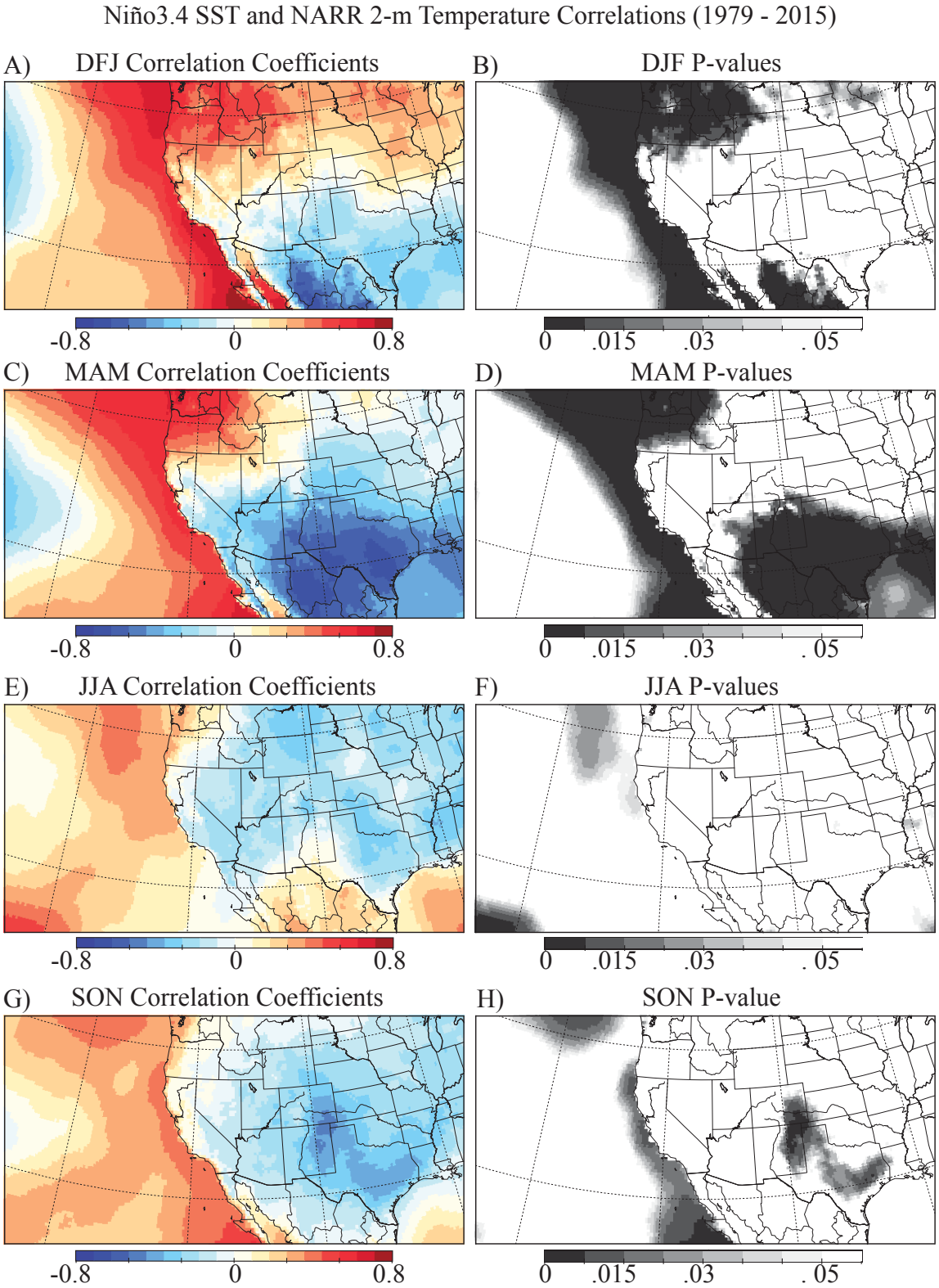

Figure 4: Niño3.4 SST and NARR 2-m temperature correlation and p-value maps (03/1979 - 11/2015). Maps represent mean correlations and p-values for the winter (A-B; December – February), spring (C-D; March – May), summer (E-F; June – August), and the fall (G-H; September – November).

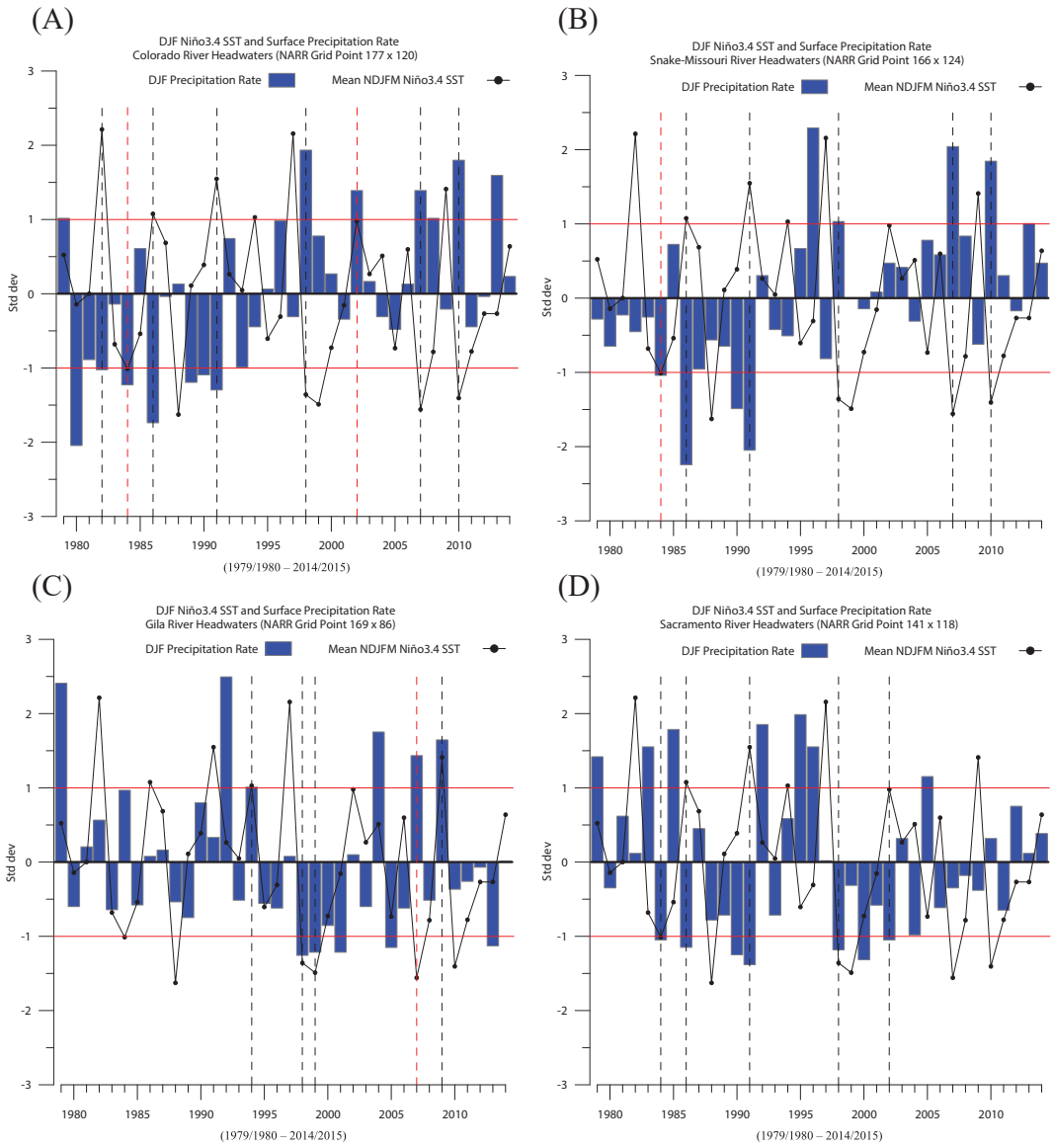

Figure 5: Mean monthly November - March Niño3.4 SST anomalies (i.e. black scatter line) and mean monthly DJF NARR surface precipitation rate (i.e. blue bars) anomalies for the Snake/Missouri River (A), Colorado River (B), Gila River (C), and Sacramento River (D) headwaters. Dashed gray and red vertical lines indicate years when both Niño3.4 SST and surface precip-itation were +/- 1sd. Dashed gray vertical lines indicate years when DJF precipitation anomalies responded to Niño3.4 SST anomalies as expected (A, B, C). Dashed red vertical lines indicate years when DJF precipitation anomalies did not respond to Niño3.4 SST anomalies as expected (A, B, C). For the Sacramento River (D), dashed gray lines were used for all years when both Niño3.4 SST and surface precipitation were +/- 1sd, as no clear correlation was identified for this headwater.

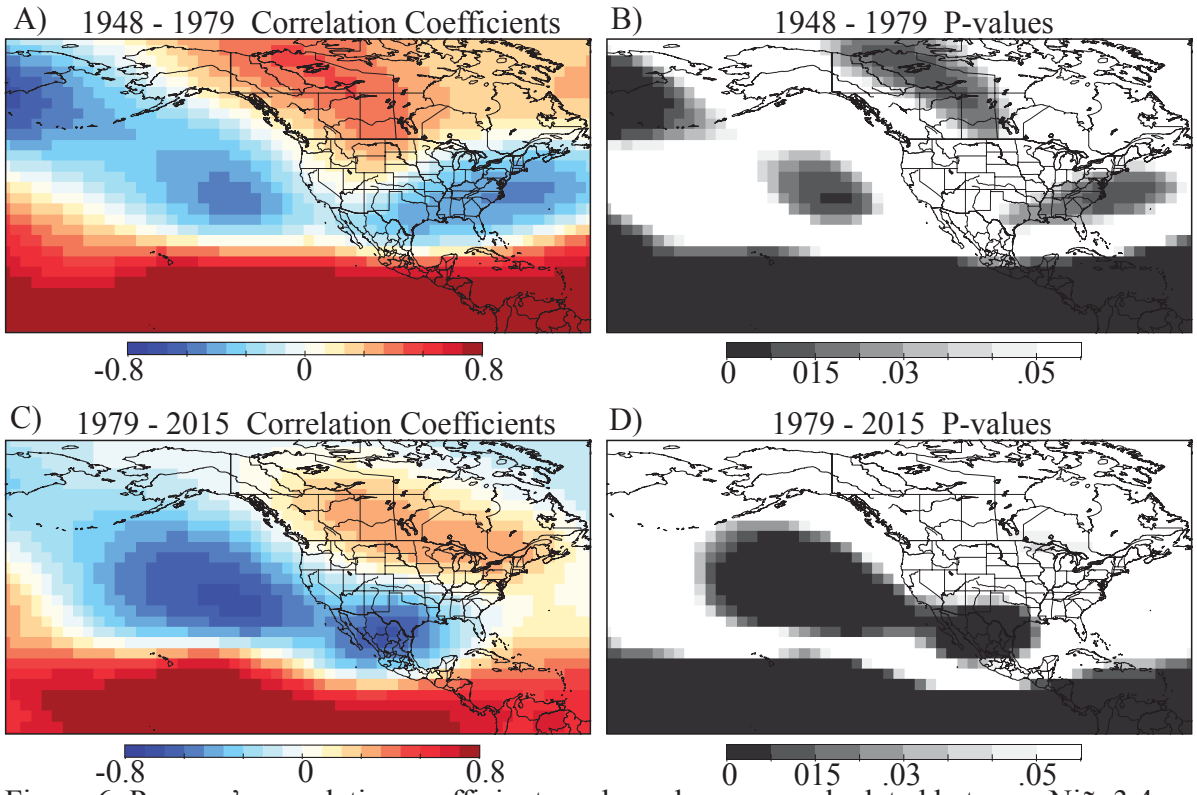

Figure 6: Pearson's correlation coefficients and p-value maps calculated between Niño3.4 SST and NARR 500mb geopotential height for time periods 12/1948 - 02/1979 (A-B) and 12/1979 - 02/2015 (C-D). Maps represent correlations and p-values for the winter season (December – February).

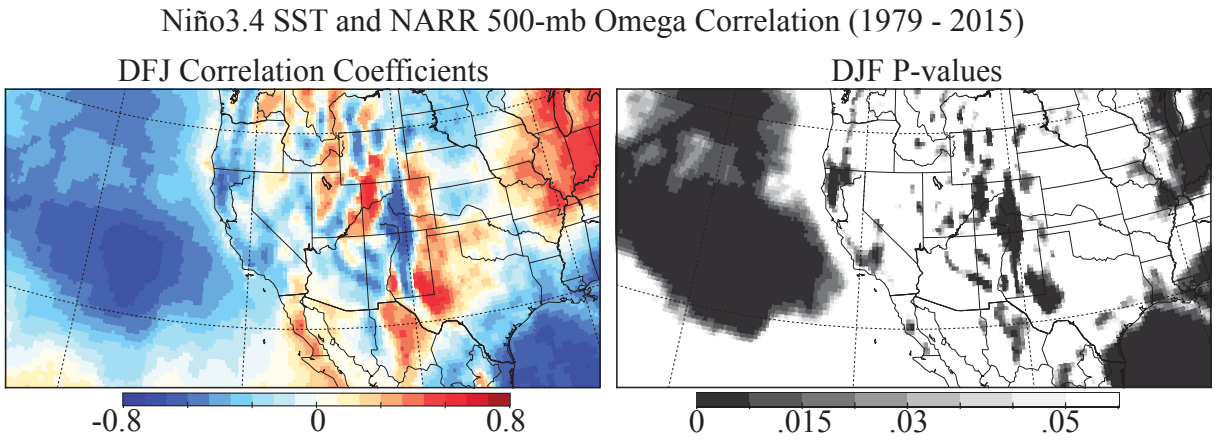

Figure 7: Pearson's correlation coefficients and p-value maps calculated between Niño3.4 SST and NARR 500mb omega (12/1979 - 02/2015). Maps represent correlations and p-values for the winter season (December – February).

DISCUSSION

Grid-point correlations performed between Niño3.4 SST and selected hydroclimate variables (Table 1) are shown in Figures 1 – 4, revealing seasonal correlation variability (Figure 1 – Figure 4), teleconnection nonstationarity (Figure 6), and atmospheric vertical velocity correlations (Figure 7). Areas are discussed in detail where grid-point correlation maps reveal significant Niño3.4 SST and western NA hydroclimate correlations, specifically over important western NA headwaters.

Our results identified Niño3.4 SST and western NA hydroclimate correlations are strongest during the cool season and DJF, and a distinct cool season and DJF correlation dipole for surface precipitation over western NA, consistent with previous research using SOI and Niño3.4 SST (e.g. Redmond and Koch 1991; Cook et al. 2010). Therefore, correlations between Niño3.4 SST and atmospheric variables in this study focused on DJF when correlations are strongest (e.g. Graham and Barnett 1994; Seager et al. 2005), and mountain snowpack important for water resources accumulates in western NA (Stewart et al. 2004; Mote et al. 2005; Barnett et al. 2008; Pederson et al. 2011). For DJF, results in important headwater regions reveal significant correlations, interannual precipitation variability (Figure 5), multidecadal teleconnection non- stationarity, and atmospheric vertical velocity over western NA.

Spatial Patterns of Correlations

Regionally, grid-point correlation maps between Niño3.4 SST and selected hydroclimate variables show spatial coherence of significant correlations (i.e. p-value < 0.05) over western NA during the cool season, DJF, and MAM (Figure 1 - Figure 4). Locally, significant correlations were observed over important headwaters during the cool season, DJF, and MAM (e.g. Colorado River in north-central Colorado), and spatial correlation variability was observed between seasons. The spatial patterns of significant correlation demonstrate spatial and temporal correlation variability.

Spatial analysis of grid-point correlation maps indicate correlation variability would be less discernable using coarser-spatial resolution climate data (e.g. NCAR/NCEP 2.5° x 2.5° grid spacing), where patterns in topographically complex regions may be obscured. Our results show areas of significant correlations at much finer spatial resolutions (e.g. DJF Niño3.4 SST and precipitation negative correlations restricted to north-central Colorado, covering an area approximately 1.5° x 1.5°). Further, spatial coherence of significant correlations (i.e. < p-value 0.05) indicates the probability that Niño3.4 SST impacts selected western NA hydroclimate variables is greater than the probability that Niño3.4 SST impacts are negligible. The homogenous patterns of correlations between Niño3.4 SST and precipitation and temperature during the cool season, DJF, and MAM indicate the correlations are correct, and not noise.

The finer-spatial resolution NARR data (0.3° x 0.3° grid spacing) illustrates spatial patterns of significant correlations within important western NA headwaters (i.e. Colorado River, Missouri River, and Snake River headwaters). Specifically, significant negative correlations between Niño3.4 SST and precipitation are visible over the upper

Colorado River, Arkansas River, Columbia River, Missouri River, and Snake River headwaters during DJF. For DJF, significant positive correlations between Niño3.4 SST and NARR precipitation are observed over the Gila River, and Río Grande in New Mexico. Significant correlations over western NA headwaters during DJF are important for climate projections of water resources. An improved understanding of central-tropical Pacific teleconnections with western NA hydroclimate can be used to evaluate climate model performance. This can be accomplished by comparing climate model outputs of future western NA hydroclimate to the spatial patterns of correlations illustrated in our grid-point correlation maps.

Seasonal Correlation Variability

Spatial analysis of Niño3.4 SST and NARR surface variables (i.e. surface precipitation rate and 2-m temperature) via correlation maps reveal seasonal correlation variability between the cool season, the warm season, DJF, MAM, JJA, and SON (Figure 1-Figure 4). For both surface variables, significant correlations over western NA are most pronounced during DJF, weaken in MAM, and are weakest during JJA and SON, with a few exceptions (e.g. 2-m temperature negative correlations strengthen over southwestern NA from DJF to MAM).

Regionally, positive correlations between Niño3.4 SST and precipitation are more concentrated over southwestern NA during MAM compared to DJF. Significant negative correlations found in the upper Colorado River, Missouri River, and Snake River headwaters during DJF, become weaker positive and negative correlations during MAM. During the warm season and JJA, significant positive correlations are seen extending from northeastern Nevada to southern Montana, areas that are impacted by convective

summer thunderstorms. Significant negative correlations during the warm season and JJA are confined to areas of central and southeastern Arizona, and extreme southwestern New Mexico. Important to note are observed significant negative correlations over areas of Arizona that are impacted by the North American Monsoon. During SON, Niño3.4 SST and precipitation positive correlations are significant over areas of western and eastern Utah, extreme western Colorado, and not significant across the rest of western NA.

Seasonal changes in correlations between Niño3.4 SST and precipitation were observed within watersheds (Figure 2A – Figure 2H). An example of seasonal correlation variability within watersheds occurs between Colorado River tributaries in western (e.g. Dolores River and Gunnison River) and north-central Colorado (e.g. Eagle River). Over the upper-Colorado River headwaters in north-central Colorado, significant negative correlations are observed during DJF, followed by weak positive correlations during MAM, and subsequent weak positive and negative correlations during JJA and SON. For western Colorado River tributaries, weak correlations are observed during DJF, strong positive correlations during MAM, weak correlations during JJA, and strong positive correlations during SON. When Niño3.4 SST are negative, wetter-than-normal DJF conditions and drier-than-normal MAM conditions typically occur over upper-Colorado River tributaries, while drier-than-normal DJF, MAM, and SON conditions could be observed over western Colorado tributaries. Positive Niño3.4 SST is typically linked with lower-than-normal DJF precipitation for upper-Colorado River tributaries and western Colorado tributaries, followed by higher-than-normal MAM precipitation for both upper and western Colorado tributaries, and higher-than-normal SON precipitation for western Colorado tributaries. Seasonal correlation variability is not limited to the Colorado River

headwaters in Colorado, and can be observed in our results over additional western NA headwaters.

Niño3.4 SST and 2-m temperature correlation variability between seasons was observed, with significant correlations observed regionally during DJF and MAM, and weak correlations observed during JJS and SON (Figure 4A – 4H). From DJF to MAM, the correlation dipole shifts northward, then weakens and becomes less apparent from MAM to JJA. Correlation maps illustrate widespread positive correlations over western NA during DJF compared to MAM. During DJF, strong positive correlations are found over the northwestern U.S., weaker positive correlations over the southwestern U.S., and strong negative correlations over areas of north-central México. Significant negative correlations strengthen and become more widespread over southwestern NA during MAM. Conversely, significant positive correlations are more concentrated over the Pacific Northwest during the MAM compared to DJF. Analogous to Niño3.4 SST and surface precipitation correlations, Niño3.4 SST and 2-m temperature correlations are weakest during the warm season, JJA, and SON. Weaker correlations in JJA and SON for both reanalysis surface variables indicates a lesser impact of Niño3.4 SST on western NA hydroclimate during the northern hemisphere summer and fall.

For the Pacific Northwest, significant positive correlations are observed during DJF and MAM, with higher-than-normal 2-m temperatures a typical response positive Niño3.4 SST. Higher-than-normal 2-m temperatures, especially in MAM, could impact headwater regions in the Pacific Northwest by reducing snowfall accumulation periods, and controlling earlier spring melt, more rapid snow melt, higher-than-normal freezing elevations, and lower-than-normal streamflow. During negative Niño3.4 SST conditions,

opposite responses compared to positive Niño3.4 SST conditions could be expected for the Pacific Northwest (e.g. lower-than-normal 2- m temperatures).

A recent shift towards more frequent positive PNA conditions (Abatzoglou 2010) is increasing the vulnerability of mountainous headwaters in the Pacific Northwest to anthropogenic climate change (Luce et al. 2013). Positive PNA conditions are generally associated with El Niño (Trenberth et al. 1998), and are important to consider for the Pacific Northwest. CMIP5 model runs suggest ENSO amplitude may increase in response to climate change and extratropical heating (Cai et al. 2014; Yamazaki and Watanabe 2015). Our results suggest an increase in ENSO amplitude could have dire consequences for areas of western NA, such as the Pacific Northwest where seasonal 2-m temperature correlations are spatially coherent (e.g. DJF to MAM). Impacts will be consistent for the Pacific Northwest across DJF and MAM, and the overall effects accumulative. If the amplitude of positive Niño3.4 SST years increases, drought conditions could be severe for this region.

Interannual DJF Correlation Variability

Overall, DJF grid-point precipitation time series for selected headwaters (Figure 5) are consistent with DJF precipitation correlation maps (Figure 2A and 2B). Both the Snake/Missouri Rivers and Colorado River headwaters time series show precipitation responding to Niño3.4 SST as expected (e.g. wetter-than-normal conditions during negative Niño3.4 SST and drier-than-normal conditions during positive Niño3.4 SST). Similarly, DJF precipitation in the Gila River headwaters responds to Niño3.4 SST as expected (e.g. wetter-than-normal conditions during positive Niño3.4 SST and drier-than-normal conditions during negative Niño3.4 SST). Consistent with DJF precipitation

correlation maps, the upper Sacramento River headwaters precipitation time series fails to show a tendency towards positive or negative anomalous conditions in response to negative or positive Niño3.4 SST.

For headwaters located in areas of weak correlations, DJF precipitation responds to Niño3.4 SST in a less predictable manner. Grid-point time series of the upper Sacramento River headwaters, crucial to water resources in northern California, shows no discernable response to Niño3.4 SST variability. From 1979 – 2015, lower-than-normal DJF precipitation during both positive Niño3.4 SST and negative Niño3.4 SST conditions were observed over the Sacramento River headwaters. No clear DJF precipitation response to Niño3.4 SST variability for the Sacramento River headwaters, and headwaters located in areas of weak correlations, complicates our ability to forecast DJF precipitation using Niño3.4 SST.

Multidecadal Teleconnection Nonstationarity

The results presented here support previous research that has identified multidecadal teleconnection nonstationary over western NA (Cole and Cook 1998; McCabe and Dettinger 1999; Hu and Feng 2001; Coats et al. 2013). Figure 6 demonstrates changes in synoptic teleconnections between Niño3.4 SST and 500mb geopotential height teleconnections during two distinct DJF time intervals (1948 – 1979 and 1979 – 2015).

Positive Niño3.4 SST forcing typically results in DJF anticyclonic flow over the northern U.S., and Canada, and cyclonic flow over southwestern NA, the eastern Pacific Ocean, and the northern Pacific Ocean. The opposite patterns are observed when Niño3.4 SST are negative. However, these patterns change over time. From 1948 – 1979, over the

southeastern U.S., DJF cyclonic flow results from positive Niño3.4 SST. From 1979 – 2015, DJF cyclonic flow shifts westward over southwestern NA as a result of positive Niño3.4 SST. DJF cyclonic flow over southwestern NA was expected from 1979 – 2015, as Niño3.4 SST and surface precipitation correlations indicate wet conditions for southwestern NA as a result of positive Niño3.4 SST.

Our results, together with previous studies (e.g. McCabe and Dettinger 1999), suggest that surface correlation variability responds to Niño3.4SST and 500mb geopotential height multidecadal teleconnection nonstationarity. Areas typically wetter-than-normal during DJF as a result of positive Niño3.4 SST from 1979 – 2015 could have experienced weaker-than-normal or opposite teleconnection signals in the past due to changes in past ENSO variability. Localized correlation variability between Niño3.4SST and surface variables (e.g. NARR 2-m temperature) are conceivable considering the teleconnection variability identified in our results, and the results of others (e.g. Coats et al. 2013). Our results suggest teleconnection variability in the northern Pacific and over NA responding to Niño3.4 SST forcing is the synoptic control on surface hydroclimate responses over western NA.

Niño3.4 SST and 500mb geopotential height teleconnections impact the fluid position of the subtropical jet stream north and south, and the displacement of the polar jet stream from east to west over Canada. For the period 1979 – 2015, during DJF negative Niño3.4 SST are associated with lower-than-normal 500mb geopotential heights centered over the northern U.S. and most of Canada, and higher-than-normal 500mb geopotential heights over the northeastern Pacific Ocean and southwestern NA. During these conditions, the polar jet stream would likely be positioned over western NA and the

northern IMW, associated with drier DJF conditions for much of the western U.S. coast and southwestern U.S. (observed in our results), and wetter DJF conditions over the northern IMW (observed in our results). For the period 1979 – 2015, positive Niño3.4 SST are associated with lower-than-normal 500mb geopotential heights over the northeastern Pacific Ocean and southwestern NA, and higher-than-normal 500mb geopotential heights over the northern U.S. and most of Canada. During these conditions, the subtropical jet stream would likely be strengthened and amplified over the eastern Pacific into southwestern NA, while the polar jet stream would likely be positioned over eastern Canada, associated with wetter conditions for southwestern NA, and drier conditions for the IMW. The synoptic controls on western NA hydroclimate shown in our results helps explain the spatial patterns of Niño3.4 SST and western NA hydroclimate grid-point correlation maps.

Atmospheric Vertical Velocity Correlations

The DJF correlation maps of Niño3.4 SST and NARR 500mb omega reveal significant correlations over important western NA headwaters (Figure 7). 500mb omega is considered here as a linking mechanism between surface-atmosphere interactions as a result of Niño3.4 SST forcing, measuring vertical velocity enhancing (i.e. uplift) or suppressing (i.e. subsidence) cloud development in the middle of the troposphere.

In general, the spatial patterns of DJF omega correlation were consistent with DJF precipitation correlations (e.g. rising motions over eastern Pacific Ocean when Niño3.4 SST are positive, rising motions over Mogollon Ridge when Niño3.4 SST are positive, or rising motions over northern Idaho and northwestern Montana when Niño3.4 SST are negative). However, the relationship between DJF omega correlations and DJF

precipitation correlations over the IMW are complex (e.g. sinking motions over upper-Colorado River headwaters when Niño3.4 SST are negative). Here we analyze the Colorado River (north-central Colorado), the Snake/Missouri River headwaters (i.e. northwest Wyoming), and the Columbia River headwaters in western Montana and northern Idaho to explore ocean-atmosphere-surface responses to Niño3.4 SST forcing over complex terrains in western NA. The position and strength of the subtropical and polar jet streams responding to Niño3.4 SST variability, and associated moisture advection and storm trajectories into western NA are considered in our analysis (e.g. Seager et al. 2005).

Rising motions over the Colorado River headwaters during DJF are expected, as wetter-than-normal DJF conditions typically result from negative Niño3.4 SST. Significant rising motions over western Colorado responding to negative Niño3.4 SST, offer one explanation for wetter-than-normal conditions over the Colorado River headwaters. When Niño3.4 SST are negative, the northerly-positioned subtropical jet stream delivers moisture, while the westerly positioned polar jet stream allows cold continental air to penetrate over the Colorado Plateau on the windward side of the Colorado Rocky Mountains (e.g. rising motions). Storms associated with the position of the polar jet stream propagate over the windward side of the continental divide, orographic lift is enhanced, and condensation occurs over the Colorado River headwaters. Strong subsidence in the atmosphere is then observed on the leeward side of the continental divide, resulting in typically drier-than-normal conditions during negative Niño3.4 SST conditions.

Rising motions over the Snake River Plain and Teton Range associated with

Niño3.4 SST support our explanation of ocean-atmosphere-surface interactions over the Colorado River headwaters. We suggest, moisture delivered via the subtropical jet stream could converge with westerly DJF storms associated with the position of the polar jet stream, enhancing frontal storm development over the Snake River Plain when Niño3.4 SST are negative. Westerly storms would be further enhanced by orographic lift over the windward side of the Teton Range, resulting in wetter-than-normal conditions over the upper Snake River and Missouri River headwaters in northwestern Wyoming. Moisture advection over areas unobstructed by topographic barriers such as the Snake River Plain supports Alexander et al. (2015), which found the Snake River Plain is a moisture pathway connected to heavy snowfall events over the Teton Range and northwestern Wyoming. Alexander et al. (2015) also found a moisture pathway unobstructed by topographic barriers via the Columbia River Plain associated with heavy snowfall events over the Rocky Mountains of northeastern Idaho and northwestern Montana. Our results show uplift and DJF precipitation are typically enhanced over the Rocky Mountains of northeastern Idaho and northwestern Montana when Niño3.4 SST are negative. We suggest enhanced DJF precipitation over the northern IMW is a function of the subtropical jet stream positioned further north (than normal), providing the polar jet stream with moisture. The polar jet stream then delivers moisture via westerly winds thru the Columbia River Plain moisture pathway, resulting in orographic lift and condensation on the windward side of the Rocky Mountains. The previously discussed 500mb rising motions over the Colorado Plateau, Snake River Plain, and Columbia River Plains are all plausible, considering the fluid position of the subtropical jet stream and associated moisture convergence with colder air associated with the westward position of the polar

jet stream during La Niña conditions (Seager et al. 2005).

Complex spatial patterns of DJF 500mb omega and Niño3.4 SST correlations over the IMW coincide with areas of weak surface (e.g. precipitation) and atmosphere (e.g. 500mb geopotential height) DJF correlations. Areas of the IMW located between the correlation dipole are characterized by overall weak DJF precipitation correlations with p-values > 0.05 (excluding Colorado River headwaters in Colorado, northern Wasatch in Utah, Snake/Missouri River headwaters in northwestern Wyoming, western Montana, and northern Idaho), weak DJF temperature correlations with p-values > 0.05 (excluding northern Wyoming, northern Wasatch range Utah, Idaho, and Montana), and weak 500mb geopotential height correlations with p- values > 0.05 (1979 – 2015). We suggest weaker correlations over the IMW can be attributed to the diverse topography impacting the variable position and strength of westerly winds and moisture advection, resulting in complex spatial patterns of 500mb omega correlations.

Modern Climate Analog

Our results illustrate the impacts Niño3.4 SST forcing can have on surface-atmosphere interactions (i.e. 500mb omega), and observed teleconnection patterns (i.e. Niño3.4 SST and 500mb geopotential height). Spatial patterns of Niño3.4 SST and 500mb omega correlations shown in this study can be used as a modern analog, similar to how pollen is used as an analog technique in paleoecology (Overpeck et al. 1985; Minckley et al. 2008). Atmospheric vertical velocity shown via Niño3.4SST and 500mb omega correlations help explain local-spatial scale climate forcing on western NA surface hydroclimate. This information is useful to climate modelers who are interested in possible mechanisms that may have impacted paleoclimatic variability. We suggest

Niño3.4 SST and 500mb omega correlations observed at fine-spatial resolutions are used to evaluate model performance of atmospheric vertical velocity in paleoclimate models of western NA hydroclimate. Similarly, such observed regional-scale atmospheric processes can be used as modern climate analogs to explain past paleoclimatic variability (Mock and Shinker 2013). Observed teleconnection patterns of Niño3.4 SST and 500mb geopotential height shown in our results are a useful modern synoptic analog. Synoptic teleconnection patterns illustrated in our results can be used to evaluate the performance of observed teleconnection patterns in paleoclimate models of NA and the eastern Pacific. We recommend paleoclimate modelers consider the local- (i.e. 500mb omega) and synoptic-scale (i.e. 500mb geopotential height) responses to Niño3.4 SST forcing shown in our study as a viable modern analog that can be used to test paleoclimate models performance, and to explain possible mechanisms of hydroclimate variability observed in paleoclimate models.

CONCLUSIONS

Grid-point correlation maps of Niño3.4 SST and selected hydroclimate variables illustrate the spatial patterns of regional and localized correlations, and their seasonal correlation variability over western NA. Further, our results are consistent with prior studies that identify strongest hydroclimate correlations during the cool season and DJF. During DJF, interannual hydroclimate variability, teleconnection nonstationarity, and surface-atmosphere interactions are observed over western NA. Seasonal correlation variability, interannual hydroclimate variability, and atmospheric vertical velocity correlations observed at fine-spatial resolutions over important headwaters have important implications for scarce water resources. Observed correlations at fine-spatial resolutions illustrate the NARR product is a viable option to detect localized western NA hydroclimate variability.

Central-tropical Pacific SST forcing impacts hydroclimate variability in western NA at regional and local spatial scales during the cool season, DJF, and MAM. Using the Niño3.4 SST and NARR hydroclimate data, spatial coherency of significant correlations are identified over important western NA headwaters during the cool season, DJF, and MAM. However, important to consider when interpreting correlation maps is DJF hydroclimate interannual variability detected via grid-point time series of four major headwaters. Overall, our spatial analysis reveals important headwaters sensitive to Niño3.4 SST and western NA hydroclimate correlation variability, with implications for

limited water resources.

Cool season and DJF hydroclimate variability is a dominant forcing on water resource variability for this region. Spatially coherent significant correlations during DJF are observed for one or more NARR reanalysis variables over important headwaters (i.e. upper Colorado River, upper Arkansas River, upper Columbia River, upper Missouri River, upper Snake River, lower Sacramento River, Gila River, lower Río Grande, and Río Conchos). However, many areas of the IMW are not characterized by significant correlations, indicating Niño3.4 SST conditions do not have a clear impact on DJF conditions in the IMW. Areas where correlations are less significant during the cool and DJF season (e.g. upper Sacramento River headwaters) are also important to consider. These areas have no clear response to Niño3.4 SST variability, with wetter- or drier-than-normal conditions observed during both positive Niño3.4 SST and negative Niño3.4 SST, or nonanomalous Niño3.4 SST conditions.

Areas of weak correlations in the IMW and interior western NA are likely impacted by varied topography, influencing large- and small-spatial scale climatic controls in the atmosphere and at the surface. Also important to consider is multidecadal teleconnection nonstationarity, which could impact the location of regional-scale atmospheric climate controls (e.g. 500mb geopotential height anomalies), altering the subtropical and polar jet streams fluid positions and associated moisture advection and storm trajectories into western NA. Further, this study identified central Tropical Pacific Ocean-atmosphere teleconnection-surface interactions. Regional (500mb geopotential teleconnection maps) and local (500mb) atmospheric controls on surface hydroclimate were explored, explaining spatial patterns of precipitation and temperature correlations

observed in our results.

The results presented here illustrate the value of using Niño3.4 SST with the fine-grid resolution NARR product to analyze hydroclimate correlations over western NA. Niño3.4 SST and reanalysis variables explored correlations consistent with prior research at regional and fine-spatial resolutions. Our results demonstrate the NARR as a viable product for future studies investigating fine-spatial hydroclimate processes in western NA. Further, information gained from NARR hydroclimate data can be used as a modern analog, to identify potential land- atmosphere interactions associated with past Niño3.4 SST variability, as well as to compare observed conditions to future model projections of western NA hydroclimate.

APPENDIX

An investigation of western NA hydroclimate correlation variability over important headwaters is possible via the fine-spatial resolution NARR product over the CONUS (i.e. 344 x 277 grid resolution over NA at 0.3°x 0.3° grid spacing over lower latitudes). While the NARR temporal resolution is shorter (i.e. 01/1979 – present) than coarser resolution GR climate data, the finer-grid resolution NARR product justifies its use in this study to capture hydroclimate variability across important western NA headwaters.

The NARR better simulates CONUS surface precipitation at finer-spatial resolutions compared to the GR. NARR precipitation data for the CONUS are disaggregated to hourly from observed 4-km WSR-88D Doppler radar data with PRISM to account for orographic effects on precipitation (Mesinger et al. 2006). For the CONUS, observed hourly gauge data are assimilated into the NARR from the National Climate Data Center daily cooperative stations (NCDC) (i.e.

8,000 reports/day), the River Forecast Center from via the Climate Prediction Center (CPC) (i.e. 7,000 reports/day), and Hourly Precipitation Data (HPD) (i.e. 2,500 reports/day) (NARR information: http://www.emc.ncep.noaa.gov/mmb/rreanl/). The NARR uses given latent heat profiles in the ETA/NOAH land surface model to simulate CONUS surface precipitation. The result is NARR model precipitation that is highly consistent with assimilated observed precipitation. Observed precipitation data

assimilated into the ETA/NOAH model validates the accuracy of simulated NARR precipitation derived from given latent heat profiles (Mesinger et al. 2006). Assimilation of observed precipitation data for the CONUS are highly consistent with hourly precipitation estimates derived from WSR-88D Doppler radar, even in topographically diverse areas such as the IMW (Mesinger et al. 2006). These results have important implications for our study, which investigates hydroclimate variability in topographically complex western NA headwaters. For México and the Oceans, Climate Prediction Center MORPHing technique (cmorph) precipitation analysis is applied (Janowiak et al. 2005). The cmorph precipitation estimates are derived from global 30-min satellite microwave (8-km) observations. Overall, modeled NARR precipitation is most accurate over the CONUS, less accurate over México and the Oceans south of 27.5°N, and least reliable over Canada and Oceans north of 42.5°N (Mesinger et al. 2006).

TOVS-1b radiance values provided by the NOAA Satellite and Information Service (i.e. NESDIS) are used to derive 2-m surface temperature (Mesinger et al. 2006). Since May 2005, 2DVAR 2-m land temperatures has been assimilated into the NARR. NARR surface temperatures demonstrate less bias and diurnal variability compared to GR2 derived surface temperatures (Mesinger et al. 2006). The accuracy of diurnal temperature cycles are improved during the winter and summer via the NARR relative to the GR2 (Mesinger et al. 2006).

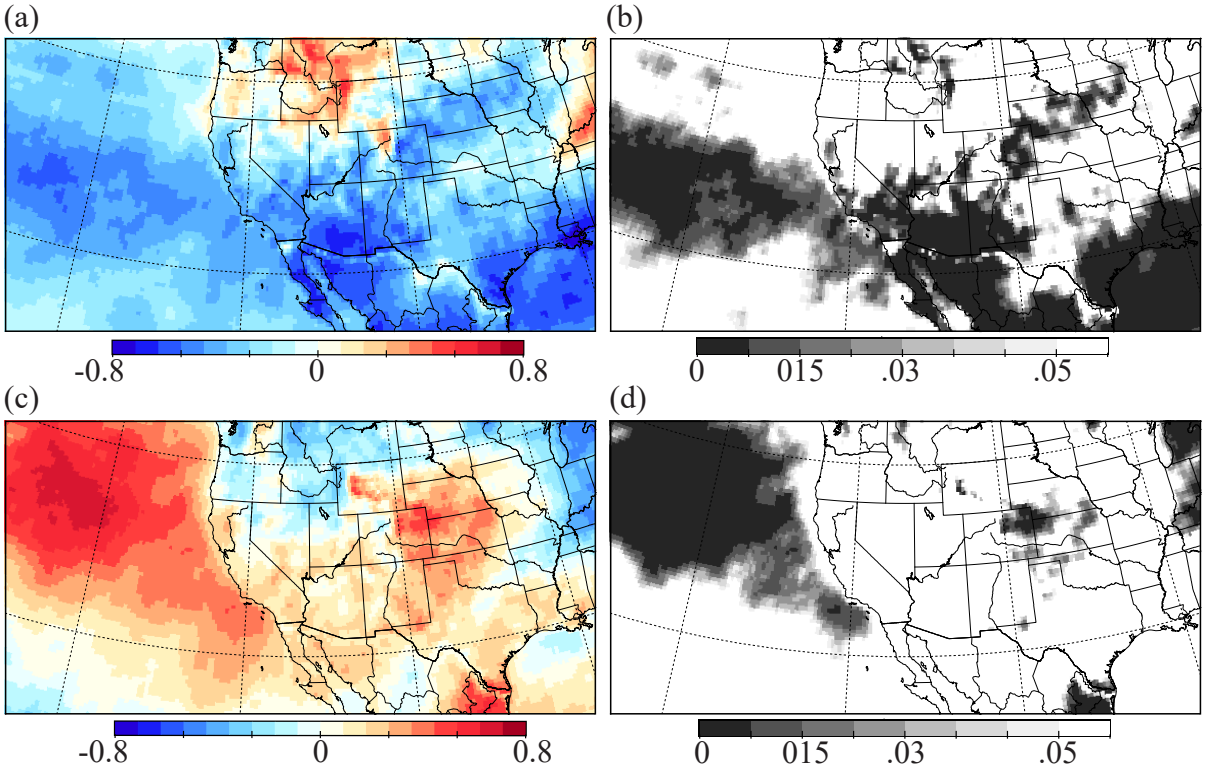

Figure 8: Pearson's correlation coefficients and p-value maps calculated between SOI (June-November) and NARR surface-precipitation rate (1979 - 2015). Maps represent correlations (A) and p-values (B) for the cool season (October – March). Pearson's correlation coefficients and p-value maps calculated between PNA and NARR surface-precipitation rate (1979 - 2015). Maps represent correlations (C) and p-values (D) for the cool season (October – March).

REFERENCES

Abatzoglou, J. T., 2010: Influence of the PNA on declining mountain snowpack in the Western United States. *Int. J. Climatol*, doi:10.1002/joc.2137.

Akima, H., 1978: A method of bivariate interpolation and smooth surface fitting for irregularly distributed data points. *ACM Transactions on Mathematical Software*, **4**, 148-159.

Alexander, M. A., J. D. Scott, D. Swales, M. Hughes, K. Mahoney, and C. A. Smith, 2015: Moisture pathways into the U.S. Intermountain West associated with heavy winter precipitation events. *J. of Hydrometeorology*, **16,** 1184-1206, doi: 10.1175/JHM-D-14- 0139.1.

Anderson, L., 2012: Rocky Mountain hydroclimate: Holocene variability and the role of insolation, ENSO and the North American Monsoon. *Global and Planetary Change*, **92- 93**,198-208, doi:10.1016/j.gloplacha.2012.05.012.

Antinao, J. L., and E. McDonald, 2013: An enhanced role for the tropical Pacific on the humid Pleistocene-Holocene transition in Southwestern North America. *Quaternary Science*, **28**, 319-341, doi:10..1016/j.quascirev.2013.03.019.

Barnett, T. P., and Coauthors, 2008: Human-induced changes in the hydrology of the Western United States. *Science,* **319**, 1080-1083.

Barron, J. A., and L. Anderson, 2010: Enhanced late Holocene ENSO/PDO expression along the margins of the eastern North Pacific. *Quaternary International*, 1-10, doi:10.1016/j.quaint.2010.02.026.

Cai, W., and Coauthors, 2014: Increasing frequency of extreme El Niño events due to greenhouse warming. *Nature Climate Change*, **4**,111-116, doi: 10.1038/NCLIMATE2100.

Cane, M. A., 2005: The evolution of El Niño, past and future. *Earth and Planetary Science Letters*, **230,** 227-240, doi:10.1016/j.epsl.2004.12.003

Castro, C. L., T. B. McKee, and R. A. Pielke Sr, 2001: The relationship of the North American Monsoon to tropical and North Pacific sea surface temperatures as revealed by observational analyses, *Bull. Amer. Meteor. Soc*, *J. Climate,* **14**, 4449-4473.

Cayan, D. R., 1996: Interannual climate variability and snowpack in the Western United States. *J. Climate*, **9**, 928-948.

Cayan, D. R., and D. H. Peterson, 1989: The influence of North Pacific atmosphere circulation on streamflow in the West. *Geophys. Monograph,* **55**, 375-397.

Cayan, D. R., K. T. Redmond, and L. G. Riddle, 1999. ENSO and hydrologic extremes in the Western United States. *J, Climate*, **12**, 2881-2893.

Chen, P., and M. Newman, 1998: Rossby wave propagation and rapid development of upper level anomalous anticyclones during the 1988 U.S. drought. *J. Climate*, **11**, 2491–2504.

Clement, A. C., R. Seager, and M. A. Cane, 2000: Suppression of El Niño during the mid-Holocene by changes in the Earth's orbit. *Paleoceanography*. **15**, 731-737.

Coats, S., J. E. Smerdon, B. I. Cook, and R. Seager, 2013: Stationarity of the tropical pacific teleconnection to North America in CMIP5/PMIP3 model simulations. *Geophy. Res. Lett.*, **40,** 4927-4932, doi: 10.1002/grl.50938.

Cole, J. E. and E. R. Cook, 1998: The changing relationship between ENSO variability and moisture balance in the continental United States. *Geophy. Res. Lett.*, **25**, 4529-4532.

Cook, B. I., R. Seager, and R. L. Miller, 2010: Atmospheric circulation anomalies during two persistent north american droughts: 1932-1939 and 1948-1957. *Climate Dyn*. doi:10.1007/s00382-010-0807-1.

Cook, B. I., J. E. Smerdon, R. Seager, S. Coats, 2014: Global warming and 21st century drying. *Climate Dyn*, doi: 10.1007/s00382-014-2075-y.

Dettinger, M. D., D.R. Cayan, G.M. Mccabe, and J.A. Marengo, 2000: Multiscale streamflow variability associated with El Niño/Southern Oscillation, in El Niño-Southern Oscillation: *Cambridge University Press*, 113 – 148.

Diaz H. F., and V. Markgraf, 2000: El Niño and the Southern Oscillation, *Cambridge University Press*.

Gershunov, A., and T. P. Barnett, 1998: ENSO influence on intraseasonal extreme rainfall and temperature frequencies in the contiguous United States: Observations and Model Results. *J. Climate*, **11**, 1575-1586.

Graham, N. E. and T. P. Barnett, 1994: ENSO and ENSO related predictability. Part II: Northern Hemisphere 700-mb height predictions based on hybrid coupled ENSO model. *J. Climate*, **8**, 544-549.

Hu, Q. and S. Feng, 2001: Variations of teleconnections of ENSO and interannual variation in summer rainfall in the Central United States. *J. Climate*, **14**, 2469-2480.

Janowiak, J. E., V. E. Kousky, and R. J. Joyce, 2005: Diurnal cycle of precipitation determined from the CMORPH high spatial and temporal resolution global precipitation analyses, *J. Geophy. Res. Atmo*., **110**(D23105), 1-18.

Kalnay, E., and Coauthors, 1996: The NCEP/NCAR 40-Year Reanalysis project. Bulletin of the American Meteorological Society, **77**, 437-471.

Kiladis, G. N., and H. F. Diaz, 1989: Global climate anomalies associated with extremes in the Southern Oscillation. *J. Climate*, **2**, 1069-1090.

Kirby, M. E., S. J. Feakins, C. A. Hiner, J. Fantozzi, S. R. H. Zimmerman, T. Dingemans, and S. A. Mensing, 2014: Tropical Pacific forcing of late-Holocene hydrologic variability in the coastal Southwestern United States. *Quaternary Science Reviews*, **102**, 27-38, doi:10.1016/j.quascirev.2014.08.005.

Kistler, R., and Coauthors, 2001: The NCEP–NCAR 50-Year Reanalysis: Monthly means CD-ROM and documentation. *Bull. Amer. Meteor. Soc*, **82**, 247- 268.

Leathers, D. J., and M. A. Palecki, 1992: The Pacific/North American teleconnection pattern and United States climate. Part II: Temporal characteristics and index specification. *J. Climate*, **5**, 707-716.

Liu, Z., Z. Lu, X. Wen, B. L. Otto-Bliesner, A. Timmermann, and K. M. Cobb, 2014: Evolution and forcing mechanisms of El Niño over the past 21,000 years. *Nature*, **515**, 550-553, doi:10.1038/ncomms4701.

Luce, C. H., J. T. Abatzoglou, and Z. A. Holden, 2013: The missing mountain water. Slower westerlies decrease orographic enhancement in the Pacific Northwest USA. *Science*, **342**, 1360-1364, doi:10.1126/science.1242335.

Mantua, N. J., and S. R. Hare, 2002: The Pacific Decadal Oscillation. *J. Oceanography*, **58**, 35- 44.

McCabe, G. J., and M. D. Dettinger, 1999: Decadal variations in the strength of ENSO teleconnections with precipitation in the Western United States. *Int. J. Climatology,* **19**, 1399-1410.

Mesinger, F., and Coauthors, 2006: North American Regional Reanalysis. *Bull. Amer. Meteor. Soc.*, **87**, 343-360, doi:10.1175/BAMS-87-3-343.

Mills, C., and J. E. Walsh, 2013: Seasonal variation and spatial patterns of the atmospheric component of the Pacific Decadal Oscillation. *J. Climate*, **26**, 1575-

1594, doi:10.1175/JCLI-D-12-00264.1.

Milly, P.C.D., J. Betancourt, M. Falkenmark, R.M. Hirsch, Z.W. Kundzewicz, D.P. Lettenmaier, and R.J. Stouffer, 2008: Stationary is dead: Whither water management? *Science,* **319**, 573-574, doi:10.1038/nature04312.

Minckley, T. A., P. J. Bartlein, C. Whitlock, B. N. Shuman, J. W. Williams, O. K. Davis. 2008: Associations among modern pollen, vegetation, and climate in Western North America. *Quaternary Science Reviews*, **27**, 1962-1991, doi:10.1016/j.quascirev.2008.07.006.

Mock, C. J., 1996: Climatic controls and spatial variations of precipitation in the Western United States. *J. Climate*, **9**, 1111-1125.

Mock, C. J., and J. J. Shinker, 2013: Modern analog approaches in paleoclimatology. *Encyclopedia of Quat. Science*, **3**, 102-112.

Moy, C. M., G. O. Seltzer, D. T. Rodbell, and D. M. Anderson, 2002: Variability of El Niño/Southern Oscillation activity at millennial timescales during the Holocene epoch. *Nature*. **420**, 162-165.

Mote, P. W., A. F. Hamlet, M. P. Clark, and D. P. Lettenmaier, 2005: Declining mountain snowpack in Western North America. *Bull. Amer. Meteor. Soc,* **86**, 39-49, doi:10.1175/BAMS-86-1-39.

Myneni, R. B., S. O. Los, and C. J. Tucker, 1996: Satellite-based identification of linked vegetation index and sea surface temperature anomaly areas from 1982 – 1990 for Africa, Australia and South America. *Geophy. Res. Lett.*, **23**, 729-732.

Newman, M., and P. D. Sardeshmukh, 1998: The impact of the annual cycle on the North Pacific/North American response to remote low-frequency forcing. *J. Atmos. Sci*., **55**, 1336–1353.

Newman, M., G. P. Compo, and M. A. Alexander, 2003: ENSO-forced variability of Pacific Decadal Oscillation. *J. Climate*, **16**, 3853-3857.

Overpeck, J.T., T. Webb III., and I. C. Prentice, 1985: Quantitative interpretation of fossil pollen spectra: dissimilarity coefficients and the method of modern analogs. *Quat. Research* **23**, 87–108.

Pederson, G. T., S. T. Gray, C. A. Woodhouse, J. L. Betancourt, D. B. Fagre, J. S. Littell, E. Watson, B. H. Luckman, and L. J. Graumlich, 2011: The unusual nature of recent snowpack declines in the North American cordillera. *Science*, **333**, 332-335, doi:10.1126/science.1201570.

Pierce, D. W., and D. R. Cayan, 2013: The uneven response of different snow measures to human-induced climate change. *J. Climate,* **26**, 4148-4167, doi: 10.1175/JCLI-

D-12- 00534.1.

Rayner N. A., D. E. Parker, E. B. Horton, C. K. Folland, L. V. Alexander, D. P. Rowell, E. C. Kent, A. Kaplan, 2003: Global analyses of sea surface temperature, sea ice, and night marine air temperature since the late nineteenth century. *J. Geophys. Res*., **108** (D14), 4407, doi:10.1029/2002JD002670.

Redmond, K. T., and R. W. Koch, 1991: Surface climate and streamflow variability in the Western United States and their relationship to large-scale circulation indices. *Water Resources Research*, **27**, 2381-2399.

Ropelewski, C. F., and M. S. Halpert, 1986: North American precipitation and temperature patterns associated with the El Niño/ Southern Oscillation (ENSO). *Mon. Wea. Rev*., **114**, 2352–2362.

R Core Team, 2015: R Studio: Integrated development for R. RStudio, Inc., Boston, MA. URL http://www.rstudio.com/

Seager, R., N. Harnik, W. A. Robinson, Y. Kushnir, M. Ting, H.-P. Huang, and J. Velez, 2005: Mechanisms of ENSO-forcing of hemispherically symmetric precipitation variability. *Quarterly J. of the Royal Meteorological Society*, **131,** 1501-1527.

Seager, R., and Coauthors, 2007: Model projections of an imminent transition to a more arid climate in Southwestern North America. *Science*, **316**, 1181-1184, doi:10.1126/science.1139601.

Seager, R., Y. Kushnir, J. Nakamura, M. Ting, and N. Naik, 2010: Northern Hemisphere winter snow anomalies: ENSO, NOA and the winter of 2009/10. *Geophy. Res. Lett.*, **37**, L14703, doi:10.1029/2010GL043830.

Seager, R., and A. Vecchi, 2010: Greenhouse warming and the 21st century hydroclimate of Southwestern North America, *Proceedings of the National Academy of Sciences*, **107**, 21277–21282.

Seager, R., M. Ting, C. Li, N. Naik, B. Cook, J. Nakamura, and H. Li, 2012: Projections of declining surface-water availability for the Southwestern United States, *Nature Climate Change*, doi:10.1038/nclimate1787.

Stewart, I, T., D. R. Cayan, and M. D. Dettinger, 2004: Changes in snowmelt runoff timing in the Western North America under a ‘business as usual’ climate change scenario. *J. Climate,* **62**, 217–232.

Shinker, J.J., P. J. Bartlein, and B. Shuman, 2006: Synoptic and dynamic climate controls of North American mid-continental aridity, *Quaternary Science Reviews*, **25**, 1401-1417, doi:10.1016/j.quascirev.2005.12.012.

Shinker, J. J., and P. J. Bartlein, 2010: Spatial variations of effective moisture in the Western United States. *Geophy. Res. Lett.*, **37**, L02701 – L02701,

doi:10.1029/2009GL041387.

Trenberth, K. E., G. W. Branstator, D. Karoly, A. Kumar, N. C. Lau, and C. Ropelewski, 1998: Progress during the TOGA in understanding and modeling global teleconnections associated with tropical sea surface temperatures. *J. Geophy. Res.*, **103**, 14,291-14,3324.

Vecchi, G. A., and A. T. Wittenberg, 2010: El Niño and our future climate: where do we stand? *WIREs Climate Change*, **1**, 260-270, doi:10.1002/wcc.33.

Verdon, D. C., A. M. Wyatt, A. S. Kiem, and S. W. Franks, 2004: Multidecadal variability of rainfall and streamflow: Eastern Australia. *Water Resources Research*, **40**, 1-8, doi:10.1029/2004WR003234.

Wallace, J. M., and D. S. Gutzler, 1981: Teleconnections in the geopotential height field during the Northern Hemisphere winter. *Bull. Amer. Meteor. Soc., Mon. Wea. Rev.*, **109**, 784- 812.

Wise, E. K., 2012: Hydroclimatology of the US Intermountain West. *Progress in Physical Geography*, **36**, 458-479, doi:10.1177/0309133312446538.

Wise, E. K., and M. P. Dannenberg, 2014: Persistence of pressure patterns over North America and the North Pacific since AD 1500. *Nature Communications*, doi:10.1038/ncomms5912.

Wittenberg, A. T., A. Rosati, T. L. Delworth, G. A. Vecchi, and F. Zeng, 2014: ENSO modulation: Is it decadally predictable? *J. Climate*, **27**, 2667-2681, doi:10.1175/JCLI-D- 13-00577.1.

Yamazaki, K., and M. Watanabe, 2015: Effects of extratropical warming on ENSO amplitudes in an ensemble of a coupled GCM. *Climate Dyn.*, **44**, 679-693, doi:10.1007/s00382-014- 2145-1.

Yarnal. B., and H. F. Diaz, 1986: Relationships between extremes of the southern oscillation and the winter climate of the Anglo-American Pacific Coast. *Inter. J. Climatology*, **6**, 197- 219.